



14 **Abstract**

15 The hippocampus is critical for memory formation. The hypothalamic supramammillary  
16 nucleus (SuM) sends long-range projections to hippocampal area CA2. While the SuM-CA2  
17 connection is critical for social memory, how this input acts on the local circuit is unknown.  
18 We found that SuM axon stimulation elicited mixed excitatory and inhibitory responses in  
19 area CA2 pyramidal neurons (PNs). We found that parvalbumin-expressing basket cells as  
20 responsible for the feedforward inhibitory drive of SuM over area CA2. Inhibition recruited  
21 by the SuM input onto CA2 PNs increased the precision of action potential firing both in  
22 conditions of low and high cholinergic tone. Furthermore, SuM stimulation in area CA2  
23 modulates CA1 activity, indicating that synchronized CA2 output drives a pulsed inhibition in  
24 area CA1. Hence, the network revealed here lays basis for understanding how SuM activity  
25 directly acts on the local hippocampal circuit to allow social memory encoding.

26

## 27 **Introduction**

28 The hippocampus is critical for memory formation and spatial navigation (Buzsáki and  
29 Moser, 2013; Eichenbaum and Cohen, 2014), yet basic questions persist regarding the  
30 circuitry and cellular components allowing these processes. While area CA2 has been shown  
31 to play a significant role in several hippocampal processes including social memory formation  
32 (Hitti and Siegelbaum, 2014; Stevenson and Caldwell, 2014) sharp-wave ripple generation  
33 (Oliva et al., 2016) and spatial encoding (Kay et al., 2016), information about the local  
34 circuitry and cellular processes allowing these functions is lacking. There is mounting  
35 evidence that generalizations cannot be made from the rich understanding of areas CA1 and  
36 CA3, as neurons in area CA2 have been shown to have unique molecular expression profiles  
37 (Cembrowski et al., 2016; Lein et al., 2004), morphology (Bartesaghi and Ravasi, 1999; No,  
38 1934) and cellular properties (Robert et al., 2020; Srinivas et al., 2017; Sun et al., 2014).  
39 Notably, and in contrast to area CA1, CA2 pyramidal neurons do not undergo NMDA-  
40 mediated synaptic plasticity (Dasgupta et al., 2020; Zhao et al., 2007). Rather, the excitability  
41 of this region is tightly controlled by a highly plastic network of inhibitory neurons (Leroy et  
42 al., 2017; Nasrallah et al., 2015; Piskorowski and Chevaleyre, 2013). When active, CA2  
43 pyramidal neurons (PNs) can strongly drive area CA1 (Chevaleyre and Siegelbaum, 2010;  
44 Kohara et al., 2014; Nasrallah et al., 2019), thereby influencing hippocampal output.  
45 Furthermore, CA2 neurons also project to area CA3, where they recruit inhibition (Boehringer  
46 et al., 2017; Kohara et al., 2014) and act to control hippocampal excitability. Thus, CA2  
47 neurons are poised to have long-reaching effects in the hippocampus, and a better  
48 understanding of the regulation of this region is needed.

49 The hypothalamic supramammillary (SuM) nucleus sends projections to both area CA2 and  
50 the dentate gyrus (Haglund et al., 1984; Vertes, 1992). These long-range connections have  
51 been shown in several species including rodents, primates and humans (Berger et al., 2001;  
52 Haglund et al., 1984; Wyss et al., 1979) where they are present in early hippocampal  
53 development. The SuM has been found to be active during a wide variety of conditions  
54 including novel environment exposure (Ito et al., 2009), reinforcement learning (Ikemoto,  
55 2005; Ikemoto et al., 2004), food anticipation (May et al., 2019), and during REM sleep and  
56 arousal (Pedersen et al., 2017; Renouard et al., 2015). This nucleus is also known for  
57 participating in hippocampal theta rhythm (Pan and McNaughton, 2002, 1997), possibly by its  
58 direct projection to the hippocampus or by modulation of the medial septum (Borhegyi et al.,  
59 1998; Vertes and Kocsis, 1997) and regulating spike-timing between hippocampus and the

60 cortex (Ito et al., 2018). Disruption of SuM neuron activity with pharmacological methods  
61 (Aranda et al., 2008; Shahidi et al., 2004) or lesions (Aranda et al., 2006) has been reported to  
62 disrupt hippocampal memory. Serotonin depletion of the SuM leads to deficiencies in spatial  
63 learning in the Morris water maze, and results in altered hippocampal theta activity  
64 (Gutiérrez-Guzmán et al., 2012; Hernández-Pérez et al., 2015). Salient rewarding experiences  
65 also activate the SuM, as evidenced by cFos expression in monoaminergic SuM neurons by  
66 consumption of rewarding food (Plaisier et al., 2020). Furthermore, the rewarding aspects of  
67 social aggression have been shown to involve an excitatory circuit between the hypothalamic  
68 ventral premammillary nucleus and the SuM (Stagkourakis et al., 2018). It has recently been  
69 shown that there are two separate populations of cells in the SuM that target either CA2 or the  
70 DG (Chen et al., 2020). In the DG, the SuM terminals release both glutamate and GABA  
71 (Boulland et al., 2009; Hashimoto et al., 2018; Pedersen et al., 2017; Soussi et al., 2010).  
72 The SuM-DG projection has been recently shown to play a role in modulating DG activity in  
73 response to contextual novelty (Chen et al., 2020) and spatial memory retrieval (Li et al.,  
74 2020). In contrast, functional studies of the SuM-CA2 projection have found that this  
75 connection is entirely glutamatergic (Chen et al., 2020). It was recently discovered that the  
76 CA2-projecting SuM neurons are active during social novelty exposure, and their selective  
77 stimulation prevents expression of a memory of a familiar conspecific (Chen et al., 2020).  
78 These findings strongly suggest that the SuM-CA2 connection conveys a social novelty signal  
79 to the hippocampus. Furthermore, recent *in vivo* recordings from the SuM in anaesthetized  
80 rats recently reported that a subset of SuM neurons were active earlier than CA2 and other  
81 hippocampal cells during SWR (Vicente et al., 2020), indicating a possible role for the SuM-  
82 CA2 projection in shaping area CA2 activity prior to SWR onset.

83 Even with the anatomical and *in vivo* data, the properties and consequences of SuM activation  
84 on area CA2 activity remain unexplored. In this study, we use a combination of approaches to  
85 specifically examine the effects of SuM input stimulation on neuronal activity in hippocampal  
86 area CA2. Here, we show that the SuM-evoked post-synaptic excitation of CA2 PN is  
87 controlled by SuM-driven inhibition. We identified PV-expressing basket cells as the  
88 neuronal population most strongly excited by SuM input in area CA2, and thus likely  
89 responsible for the feedforward inhibition evoked by SuM in CA2 PNs. We found that  
90 recruitment of this inhibition enhances the precision of AP firing by area CA2 PNs in  
91 conditions of low and high cholinergic tone. Finally, we observed that the resulting  
92 synchronized CA2 PN activity drives inhibition in area CA1, thereby providing a circuit

93 mechanism through which SuM can modulate hippocampal excitability by controlling area  
94 CA2 output.

95

## 96 **Results**

97 In order to functionally investigate the SuM projection to area CA2, we used an anterograde  
98 strategy in two separate transgenic mouse lines (Figure 1A and Supplemental Figure 1F). It  
99 has been shown that the source of vesicular glutamate transporter 2 (VGLUT2)-  
100 immunopositive boutons in area CA2 originate from the SuM (Halasy et al., 2004). To further  
101 assess where these VGLUT2-expressing SuM cells project into the hippocampus, we injected  
102 an AAV to express channelrhodopsin(H143R)-YFP (ChR2-EYFP) under the control of Cre  
103 into the SuM of a transgenic mouse line with Cre expression controlled by the VGLUT2  
104 promoter, the Tg(Slc17ab-icre)10Ki line (Borgius et al., 2010) (Supplemental Figure 1F). In  
105 parallel, we used a novel mouse line, the Csf2rb2-Cre line that selectively expresses Cre in  
106 the SuM (Chen et al., 2020) (Figure 1A). To find the optimal injection site, we injected a  
107 retrograde canine adenovirus type 2 (CAV-2) into area CA2 of the hippocampus to permit the  
108 expression of Cre-recombinase (Cre) in hippocampal-projecting SuM neurons, and an adeno-  
109 associated virus (AAV) was injected into the SuM to allow the expression of EGFP under the  
110 control of Cre (Supplemental Figure 1A). In 5 animals the injection of retrograde CAV-2 was  
111 sufficiently targeted to area CA2, as indicated by the presence of EGFP-expressing SuM  
112 axonal fibers primarily in this hippocampal area (Supplemental Figure 1B). We stained for  
113 calretinin to define the boundaries of the SuM nucleus (Pan and Mcnaughton, 2004).  
114 Consistent with what has been described (Chen et al., 2020), we observed that CA2-projecting  
115 cells co-express calretinin and are located in the medial SuM (Supplemental figure 1C-D).  
116 These cells were located bilaterally, ventral to the fiber bundles that traverse the SuM  
117 (Supplemental Figure 1C).

118 We found that with both transgenic mouse lines we could reproducibly restrict expression of  
119 ChR2-EYFP in the SuM and avoid infecting nearby hypothalamic regions that also may  
120 project to the hippocampus (Figure 1A, Supplemental Figure 1F). For all experiments,  
121 injection sites were examined post hoc to ensure correct targeting of the SuM. With both lines  
122 of transgenic mice, we observed identical patterns of SuM fiber localization in the  
123 hippocampus. EYFP-containing SuM axons were found throughout the supragranular layer of  
124 the DG and in area CA2 (Figure 1B) where they clustered around the pyramidal layer

125 (stratum pyramidale, SP) and spread in stratum oriens (SO). The SuM fiber projection area  
126 was clearly restricted to area CA2, as defined by expression of the CA2-specific markers  
127 PCP4 and RGS14 and did not spread to neighboring areas CA3 and CA1 (Figure 1B). In  
128 order to maximize the precision of our experiments, we frequently only achieved partial  
129 infection of the SuM, as indicated by the sparseness of Chr2-EYFP-containing fibers in  
130 comparison to the number of vGluT2-stained boutons in this region (Supplemental Figure 1G-  
131 H).

### 132 SuM axons provide excitatory glutamatergic input to pyramidal neurons in area CA2 and 133 CA3a

134 In order to better understand the cellular targets and consequences of SuM input activity in  
135 area CA2, we applied the above experimental strategy to express Chr2-EYFP in SuM axonal  
136 fibers and performed whole-cell current and voltage clamp recordings of PNs across the  
137 hippocampal CA regions and activated projecting axons with pulses of 488 nm light in acute  
138 hippocampal slices. Following all recordings, we performed post-hoc anatomical  
139 reconstructions of recorded cells and axonal fibers, as well as immunohistochemical staining  
140 for CA2-area markers.

141 We observed that photostimulation of SuM axons elicited excitatory post-synaptic responses  
142 in 63 % of PNs (n = 166 of 263 cells) located in area CA2. PNs in this region shared similar  
143 overall dendritic morphologies and electrophysiological properties (Table 1) but differed  
144 along two criteria. First, in *stratum lucidum* some PNs clearly had thorny excrescences (TE)  
145 while others had very smooth apical dendrites (Figure 1C-D). Based on the presence of TEs,  
146 we classified cells as CA2 or CA3 PNs (unequivocal distinction was possible for 148  
147 neurons). Second, the distribution locations of PN soma along the radial axis of the  
148 hippocampus allowed us to cluster them as deep (closer to *stratum oriens*, SO) or superficial  
149 (closer to *stratum radiatum*, SR) subpopulations (unequivocal distinction was possible for 157  
150 neurons). We found that the SuM-PN connectivity was not different between CA2 and CA3  
151 PNs (Table 2,  $\chi^2$  test for CA2 and CA3 PNs,  $p = 0.572$ ) or between deep and superficial PNs  
152 (Table 2,  $\chi^2$  test for deep and superficial PNs,  $p = 0.946$ ). Light-evoked excitatory post-  
153 synaptic potentials (EPSPs) and excitatory post-synaptic currents (EPSCs) recorded at -70mV  
154 were of fairly small amplitude (Figure 1C and 1D) that were similar regardless of the PN type  
155 or somatic location (Table 2, Mann-Whitney U test for CA2 and CA3 PNs,  $p = 0.409$ ; Mann-  
156 Whitney U test for deep and superficial PNs,  $p = 0.306$ ). Because no significant differences in  
157 post-synaptic responses to SuM input stimulation were observed between CA2 and CA3 PNs

158 as well as between deep and superficial PNs, data from all PNs was pooled for the rest of the  
159 study. The small amplitude of SuM input-evoked post-synaptic responses in PNs was not due  
160 to under-stimulation of SuM axons as EPSC amplitudes rapidly reached a plateau when  
161 increasing light intensity (Supplemental Figure 2). We are confident that this transmission is  
162 due to action potential-generated vesicle release because all transmission was blocked  
163 following application of tetrodotoxin (TTX) (Supplemental Figure 2). The pure glutamatergic  
164 nature of the SuM input was confirmed by the complete block of light-evoked synaptic  
165 transmission following the application of NBQX and D-APV (Supplemental Figure 2;  
166 amplitudes were  $16 \pm 4.8$  pA in control and  $1.8 \pm 0.3$  pA in NBQX & D-APV,  $n = 6$ ;  
167 Wilcoxon signed-rank test,  $p = 0.03$ ). These data confirm that SuM inputs provide long-range  
168 glutamatergic excitation to CA2 and CA3 PNs in area CA2.

#### 169 PNs in area CA2 receive mixed excitatory and inhibitory responses from SuM input

170 Photostimulation of SuM input elicited excitatory post-synaptic potentials (EPSPs) of fairly  
171 small amplitude in area CA2 PNs held at  $-70$  mV (Figure 1E and 1F). Because current clamp  
172 experiments also show that SuM stimulation input also recruits feedforward inhibition in area  
173 CA2 (Figure 1 C4 and D4), we asked if the amplitude of SuM input stimulation-evoked  
174 EPSPs in PNs could be controlled by inhibition. Interestingly, blocking inhibitory  
175 transmission with the GABA<sub>A</sub> and GABA<sub>B</sub> receptor antagonists SR95531 and CGP55845A  
176 led to a significant increase of light-evoked EPSP amplitude recorded in area CA2 PNs  
177 (Figure 1F and 1G; amplitudes of the first response were  $0.18 \pm 0.05$  mV in control and  $0.24$   
178  $\pm 0.05$  mV in SR95531 & CGP55845A,  $n = 14$ ; Wilcoxon signed-rank tests,  $p = 0.004$  for the  
179 first PSP,  $p = 0.013$  for the second PSP,  $p < 0.001$  for the third PSP). Thus, this result  
180 demonstrates a negative control of SuM-driven excitation by feedforward inhibition.

#### 181 Basket cells are strongly recruited by SuM inputs

182 Because the hippocampus hosts a variety of interneurons (INs) that are involved in controlling  
183 specific aspects of PN excitability, we wished to establish which kind of IN was targeted by  
184 the SuM input to area CA2. We performed whole-cell recordings from INs in this area and  
185 assessed post-synaptic excitatory responses to SuM axons stimulation in these cells (Figure  
186 2). In contrast with previous reports of an exclusive innervation of PNs by SuM (Maglóczy  
187 et al., 1994), we observed robust light-evoked excitatory transmission from SuM axons in 35  
188 out of 62 interneurons (INs) with soma located in SP. Following anatomical biocytin-  
189 streptavidin staining and reconstructions of recorded INs (allowing unequivocal identification  
190 in 48 neurons), we were able to classify INs based on their physiological properties, somatic



191 location and axonal arborization location. We classified 22 cells as basket cells (BCs) because  
192 their axonal arborizations were restricted to SP (Figure 2A). BCs fired APs at high frequency  
193 either in bursts or continuously upon depolarizing current injection and showed substantial  
194 repolarizing sag current when hyperpolarized (Table 3). Light-evoked EPSCs and EPSPs  
195 were readily observed in the vast majority of BCs (Figure 2A and C, Table 4) and reached  
196 large amplitudes in some instances. An additional 26 INs with soma in SP were classified as  
197 non-BCs because their axon did not target SP (Figure 2B). In our recordings, these cells fired  
198 in bursts and showed little sag during hyperpolarizing current injection steps (Table 3). We  
199 consistently observed no or very minor light-evoked excitatory transmission onto non-BCs  
200 (Figure 2C, Table 4). Furthermore, we recorded from 17 INs that had soma in stratum oriens  
201 (SO) and 9 in stratum radiatum (SR). Like non-BCs, these INs did not receive strong  
202 excitation from SuM fibers (Table 4). This data is consistent with the conclusion that SuM  
203 input preferentially forms excitatory synapses onto basket cells in area CA2.

204 To fully assess the strength of SuM inputs onto the different cell types, we examined the  
205 following parameters for each population: the connectivity, success rate, amplitude, potency,  
206 kinetics, and latencies of EPSCs as well as the resulting depolarization of the membrane  
207 potential. First, SuM inputs preferentially innervated BCs as evidenced by a higher  
208 connectivity of EPSCs in BCs than in PNs or other INs (Table 4). Importantly, excitatory  
209 responses had short latencies with limited jitter (Table 4) indicating that the connection was  
210 monosynaptic in all cell types. When voltage-clamping cells at -70 mV, light-evoked EPSCs  
211 could be compared between different cell populations. However, not every photostimulation  
212 gave rise to an EPSC leading to an average success rate that tended to be highest in BCs  
213 (Table 4). In addition, BCs appeared to receive more excitation from SuM inputs than other  
214 cells types, as the amplitude of EPSCs were larger in BCs than in PNs (Table 4). EPSCs  
215 recorded in BCs also had faster kinetics than in PNs (Table 4). Interestingly, combining the  
216 success rate of EPSCs with their respective amplitudes to compute the potency of the SuM  
217 synapses revealed that it was significantly larger in BCs than in PNs and non-BCs (Figure 2C;  
218 potencies were  $12 \pm 1.6$  pA for PNs,  $n = 166$ ;  $29 \pm 7.8$  pA for BCs,  $n = 18$ ;  $5.9 \pm 1.5$  pA for  
219 non-BCs,  $n = 13$ ; Kruskal-Wallis test with Dunn-Holland-Wolfe post hoc test,  $p = 0.022$ ).  
220 Consequently, EPSPs recorded at -70 mV were of larger amplitude in BCs than in PNs and  
221 non-BCs (Figure 2D; amplitudes were  $0.44 \pm 0.06$  mV for PNs,  $n = 20$ ;  $1.71 \pm 0.57$  mV for  
222 BCs,  $n = 10$ ;  $0.53 \pm 0.07$  mV for non-BCs,  $n = 4$ ; Kruskal-Wallis test with Dunn-Holland-  
223 Wolfe post hoc test,  $p < 0.001$ ). When recording cell-attached or current-clamping BCs at



224 their resting membrane potential ( $V_M$ ), photostimulation of SuM axons was able to evoke AP  
225 firing (Figure 2E) in multiple instances ( $n = 7$  of 13), this was never observed in PNs ( $n = 0$  of  
226 78), non-BCs ( $n = 0$  of 16), SR INs ( $n = 0$  of 9) or SO INs ( $n = 0$  of 8). These results show  
227 that SuM projections to area CA2 preferentially provide excitation to BCs that are likely  
228 responsible of the feedforward inhibition observed in PNs. This is in accordance with an  
229 efficient control of area CA2 PNs excitation by the SuM inhibitory drive as axons from BCs  
230 deliver the feedforward inhibition to the peri-somatic region of PNs.

### 231 Parvalbumin-expressing basket cells mediate the feedforward inhibition recruited by SuM

232 In the hippocampus, BCs express either cholecystokinin (CCK) or parvalbumin (PV)  
233 (Klausberger and Somogyi, 2008). We found that in response to a 1 second depolarizing  
234 pulse, most BCs that received strong SuM excitatory input displayed very fast AP firing with  
235 little accommodation in the AP firing frequency (Table 3, Figure 3A and B). This firing  
236 behavior is similar to what has been reported for fast spiking PV-expressing BCs in CA1  
237 (Pawelzik et al., 2002). In contrast, CCK-expressing BCs show a lower firing frequency and  
238 more accommodation during the train (Pawelzik et al., 2002). This result suggests that BCs  
239 connected by the SuM may be expressing PV. To directly confirm this hypothesis, we  
240 performed post-hoc immunostaining of recorded interneurons that received strong excitation  
241 from SuM input. Because of the dialysis inherent to the whole-cell recording conditions, we  
242 encountered difficulty staining for multiple cells. However, PV-immunoreactivity could  
243 unequivocally be detected in either the soma or dendrites of 7 connected BCs (Figure 3C).  
244 Therefore, this data demonstrates that at least a fraction of the recorded BCs connected by the  
245 SuM are expressing PV.

246 Hence, to address whether the lack of PV staining in some cells was a consequence of dialysis  
247 or resulted from the fact that non-PV BC are also connected, we made use of a different  
248 strategy to differentiate PV and CCK INs. It has previously been demonstrated that PV+ BC  
249 transmission can be strongly attenuated by mu opioid receptor activation (MOR) while CCK+  
250 BC transmission is insensitive to MOR activation (Glickfeld et al., 2008). Thus, in order to  
251 determine if SuM inputs preferentially target one subpopulation of BCs, we recorded from  
252 PNs in area CA2 and examined the sensitivity of light-evoked IPSCs to the application of the  
253 MOR agonist DAMGO (Figure 4A). We found that there was a near complete block of the  
254 light-evoked IPSC amplitude following 1  $\mu$ M DAMGO application (Figure 4A; IPSC  
255 amplitudes were  $343 \pm 123$  pA in control and  $31 \pm 12.4$  pA in DAMGO hence a  $88 \pm 5.0$  %  
256 block by DAMGO,  $n = 6$  PNs; Wilcoxon signed-rank test,  $p = 0.031$ ), while direct excitatory

257 transmission remained unaffected (Figure 4A; EPSC amplitudes were  $6.7 \pm 1.1$  pA in  
258 SR95531 & CGP55845A and  $5.6 \pm 0.9$  pA after DAMGO,  $n = 17$  PNs; Wilcoxon signed-rank  
259 test,  $p = 0.19$ ).

260 Because a fraction of PV+ INs in area CA2 is also the substrate of an iLTD of feedforward  
261 inhibition from CA3 mediated by delta opioid receptor (DOR) activation, we sought to further  
262 refine our characterization of the SuM feedforward inhibition by assessing its sensitivity to  
263 DOR activation. Application of  $0.5 \mu\text{M}$  of the DOR agonist DPDPE led to a long-term  
264 reduction of light-evoked IPSCs recorded in area CA2 PNs, similar to the iLTD seen by CA3  
265 input stimulation (Figure 4B; amplitudes were  $168 \pm 28$  pA in control and  $64 \pm 22$  pA in  
266 DPDPE hence a  $61 \pm 14$  % block by DPDPE,  $n = 7$ ; paired-T test,  $p = 0.015$ ), while leaving  
267 direct EPSCs unaffected (Figure 4B; amplitudes were  $4.0 \pm 1.6$  pA in SR95531 &  
268 CGP55845A and  $3.1 \pm 1.1$  pA after DPDPE,  $n = 7$ ; Wilcoxon signed-rank test,  $p = 0.22$ ).  
269 Further confirming the PV+ nature of INs responsible for the SuM feedforward inhibition,  
270 this result reveals that both the local CA3 and long-range SuM inputs converge onto the same  
271 population of INs to inhibit area CA2 PNs, thus enabling cross-talk between these routes  
272 through synaptic plasticity of PV+ INs.

273 Following up on this observation, we wished to genetically confirm that PV+ INs are  
274 responsible for the SuM feedforward inhibition over area CA2 PNs. As the dichotomy  
275 between PV+ versus CCK+ INs sensitivity to opioids has not been directly verified in area  
276 CA2, we used inhibitory DREADD to selectively inhibit PV+ INs in area CA2 while  
277 monitoring feedforward IPSCs from area CA2 PNs in response to SuM stimulation. To  
278 achieve that, we injected AAVs expressing a Cre-dependent h4MDi inhibitory DREADD in  
279 area CA2 of PV-Cre mice together with AAVs expressing ChR2 with a pan-neuronal  
280 promoter in the SuM (Figure 4C). We observed a substantial reduction of SuM-evoked IPSC  
281 amplitude recorded in area CA2 PNs upon application of  $10 \mu\text{M}$  of the DREADD ligand  
282 CNO (Figure 4D; amplitudes were  $847 \pm 122$  pA in control and  $498 \pm 87$  pA in CNO hence a  
283  $42 \pm 6.0$  % block by CNO,  $n = 13$ ; paired-T test,  $p < 0.001$ ). Although we never measured a  
284 complete block of inhibitory responses, this result unequivocally places PV+ INs as mediators  
285 of the SuM feedforward inhibition of area CA2 PNs. The incomplete block of IPSCs in these  
286 experiments could be a consequence of partial infection of PV+ INs in area CA2 by AAVs  
287 carrying DREADDs (Figure 4E; fraction of PV+ INs expressing DREADDs in CA2 =  $75 \pm$   
288  $3.5$  %,  $n = 13$ ) and partial silencing of DREADD-expressing PV+ INs by CNO. Altogether,

289 these combined results strongly indicate that SuM axons are efficiently and selectively  
290 exciting PV+ BCs in area CA2, thus driving a feedforward inhibition onto neighboring PNs.

### 291 The feedforward inhibitory drive from SuM controls pyramidal neurons excitability

292 Given SuM axonal stimulation triggers an excitatory-inhibitory sequence in post-synaptic  
293 PNs, we asked which effect would prevail on PN excitability. In order to assess this, we  
294 mimicked an active state in PNs by injecting constant depolarizing current steps sufficient to  
295 sustain AP firing during 1 second while photostimulating SuM axons at 10 Hz (Figure 5A and  
296 5B). We observed that recruitment of SuM inputs significantly delayed the onset of the first  
297 AP (Figure 5C; latency to the first AP were  $221 \pm 19.9$  ms in control and  $233 \pm 19.1$  ms with  
298 photostimulation, hence a  $12.1 \pm 4.3$  ms increase upon photostimulation,  $n = 12$ ; paired-T test,  
299  $p = 0.016$ ). In addition, given SuM neurons display theta-locked firing *in vivo*, we asked if  
300 rhythmic inhibition driven by SuM inputs in area CA2 could pace AP firing in PNs by  
301 defining windows of excitability. Indeed, photostimulation of SuM axons at 10 Hz led to a  
302 significant decrease of variability in the timing of AP firing by PNs (Figure 5D and 5E;  
303 standard deviations of the first AP timing were  $36.9 \pm 11$  ms in control and  $24.7 \pm 7.4$  ms with  
304 photostimulation, hence a  $12.3 \pm 5.3$  ms decrease upon photostimulation,  $n = 12$ ; Wilcoxon  
305 signed-rank tests,  $p < 0.001$  for the first AP,  $p = 0.008$  for the second AP,  $p = 0.004$  for the  
306 third AP). Both the delay of AP onset and the reduction of AP jitter stemmed from the  
307 feedforward inhibition recruited by SuM inputs as application of GABA<sub>A</sub> and GABA<sub>B</sub>  
308 receptor antagonists abolished these effects of SuM stimulation (Figure 5C-E; latency to the  
309 first AP were  $232 \pm 19.8$  ms in SR95531 & CGP55845A and  $235 \pm 18.0$  ms with  
310 photostimulation,  $n = 6$ ; Wilcoxon signed-rank test,  $p = 0.44$ ; standard deviations of the first  
311 AP timing were  $11.9 \pm 2.0$  ms in SR95531 & CGP55845A and  $7.1 \pm 1.5$  ms with  
312 photostimulation,  $n = 6$ ; Wilcoxon signed-rank tests,  $p = 0.22$  for the first AP,  $p = 0.16$  for the  
313 second AP,  $p = 0.09$  for the third AP). These results reveal that the purely glutamatergic SuM  
314 input, by recruiting feedforward inhibition, has an overall inhibitory effect on PN excitability  
315 and can influence the timing and jitter of area CA2 PN action potential firing.

316 It has been reported that the AP discharge of SuM neurons *in vivo* is phase-locked to the  
317 hippocampal theta rhythm (Kocsis and Vertes, 1994). Because theta rhythm is a brain state  
318 characterized by elevated levels of acetylcholine, we approximately mimicked these  
319 conditions in the hippocampal slice preparation by bath application of 10  $\mu$ M of the  
320 cholinergic agonist carbachol (CCh). Under these conditions, CA2 PNs depolarize and  
321 spontaneously fire rhythmic bursts of APs, and the properties of these AP bursts are tightly

322 controlled by excitatory and inhibitory synaptic transmission (Robert et al., 2020). Of note,  
323 we observed that CCh application depressed the SuM-CA2 excitatory and inhibitory drive and  
324 decreased short-term depression at these synapses (Supplemental Figure 3). Under these  
325 conditions, we asked how this spontaneous AP bursting activity would be affected by  
326 activation of the SuM input by triggering 10 second-long trains of 0.5 ms light pulses  
327 delivered at 10 Hz to stimulate SuM axons at the onset of bursts (Figure 6A). Because of the  
328 intrinsic cell-to-cell variability of bursting kinetics, we photo-stimulated SuM inputs only  
329 during interleaved bursts in the same cells. To do this, bursts were detected automatically  
330 with an online threshold detection system that started the photostimulation pulse train after  
331 the first AP of every alternating burst, starting with the second burst (Figure 6A and B). For  
332 analysis, the number of APs and bursting kinetics could be compared within the same cell.  
333 We observed a significant decrease in the number of APs fired during a burst when SuM  
334 inputs were photo-stimulated as compared to interleaved control bursts (Figure 6C and 6D;  
335 numbers of APs per burst were  $15.2 \pm 2.3$  in control and  $6.9 \pm 1.3$  with photostimulation,  $n =$   
336  $7$ ; paired-T test,  $p = 0.031$ ). In control bursts, the AP firing rate of CA2 PNs initially  
337 increases, and then progressively decreases. In the photo-stimulation bursts, the initial  
338 increase of AP firing frequency was absent, and the subsequent AP firing frequency was  
339 reduced (Figure 6E; 2-way ANOVA on firing rate over time in light-on vs light-off  
340 conditions; light factor,  $p < 0.001$ ; time factor,  $p < 0.001$ ; light x time factor,  $p = 0.052$ ).

341 In the presence of CCh, spontaneous AP bursting is preceded by a membrane depolarization.  
342 Following several seconds of AP firing, the membrane potential of CA2 PNs remains  
343 depolarized for several seconds, and slowly hyperpolarizes until the next burst event. We  
344 observed that photo-stimulation of SuM inputs resulted in a striking reduction in the amount  
345 of time the membrane potential remained depolarized, and this is likely why the burst  
346 duration was significantly shorter in bursts with SuM photo-stimulation (Figure 6F and G;  
347 burst duration was  $4.0 \pm 1.1$  s in control and  $1.6 \pm 0.5$  s with photostimulation,  $n = 7$ ; paired-T  
348 test,  $p = 0.037$ ). The rate and level of  $V_M$  repolarization following bursts were not  
349 significantly changed by SuM input photostimulation ( $V_M$  repolarization rate was  $-3.3 \pm 0.6$   
350 mV/s in control and  $-3.6 \pm 0.7$  mV/s with photostimulation,  $n = 7$ ; paired-T test,  $p = 0.601$ ;  
351 post-burst  $V_M$  was  $-62.8 \pm 1.7$  mV in control and  $-62.0 \pm 2.0$  mV with photostimulation,  $n =$   
352  $7$ ; paired-T test,  $p = 0.173$ ), however the inter-burst time interval was reduced. Indeed, AP  
353 bursts with SuM input activation were followed more rapidly by another burst of AP than the  
354 ones without SuM input activation (Figure 6B, H; time until next burst was  $93 \pm 14$  s in

355 control and  $59 \pm 17$  s with photostimulation,  $n = 7$ ; paired-T test,  $p = 0.001$ ), which could be  
356 due to both short-term depression of inhibitory transmission after repeated activation during  
357 the SuM input photostimulation train and reduced activation of hyperpolarizing conductances  
358 during bursts shortened by SuM input photostimulation. Thus, in our preparation, SuM input  
359 activation is able to modify the spontaneous bursting activity of CA2 PNs under conditions of  
360 high cholinergic tone.

361 As SuM input controls burst firing of action potentials and likely paces activity in area CA2,  
362 we wondered how the subsequent output of CA2 PNs would affect their post-synaptic targets.  
363 Because CA2 PNs strongly project to CA1 PNs, this activity is likely to influence CA1  
364 encoding and hippocampal output. Thus, we examined the consequences of SuM-CA2 input  
365 stimulation on area CA1 both in vivo and in acute slices treated with CCh to induce  
366 spontaneous activity (Figure 7).

367 ChR2-EYFP was expressed in the SuM of *Csf2rb2-cre* mice in a cre-dependent manner and  
368 the mice were implanted with a microdrive targeting tetrodes to region CA1 and an optical  
369 fiber to the SuM terminals in CA2 (Figure 7A). Mice were placed in a small box (familiar  
370 context) and left free to explore as blue (473 nm) laser light pulses (50 ms pulse width) were  
371 applied to the SuM terminals at 10 Hz. Across 23 recording sessions in five mice we found  
372 that the activation of SuM terminals in CA2 resulted in a significant and reproducible change  
373 in the multiunit spiking activity recorded in the pyramidal cell layer of CA1 on 34 of 55  
374 tetrodes. The firing rate change was similar across individual tetrodes (Figure 7B and C), with  
375 a decrease in the normalized firing rate starting shortly after laser onset and continuing for  
376 about 10 ms, followed immediately by a rebound-like increase to about 20 % greater than  
377 baseline firing rate (Figure 7B and C).

378 In order to get a better mechanistic understanding of this observation, we set out to decipher  
379 how SuM activity in area CA2 influences CA1 in the hippocampal slice preparation. To this  
380 end, we used the same photostimulation protocol used in vivo that consisted of light  
381 stimulation trains of 50 ms-long pulses delivered at 10 Hz for 1 second, repeated every 10  
382 seconds for 2 minutes and interleaved with light-off sweeps of the same duration, with the  
383 microscope objective centered on area CA2. Whole-cell patch-clamp recordings of CA1 PNs  
384 were obtained in acute hippocampal slices superfused with CCh and subjected to this light  
385 stimulation protocol (Figure 7D). We asked what synaptic events may be responsible for the  
386 decreased firing of CA1 units observed 10 – 20 ms after light onset in vivo (Figure 7A-C).  
387 Whole-cell recordings of CA1 PNs showed an absence of EPSCs time-locked to the

388 photostimulation in all but one case (n = 11/12) (Figure 7E and F). In contrast, we often (n =  
389 7/12) observed light-evoked IPSCs in CA1 PNs occurring 10 – 20 ms after light onset (Figure  
390 7G and H). Therefore, the reduction in firing of CA1 units in vivo is likely caused by  
391 increased inhibitory inputs onto CA1 PNs within 10 – 20 ms of SuM fiber stimulation over  
392 area CA2. This result highlights a contribution of SuM input to controlling CA2 output that  
393 regulate CA1 activity in vivo and provides a mechanistic interpretation of this observation at  
394 the circuit level.

395

## 396 **Discussion**

397 In this study, we provide direct evidence for a functional connection between the  
398 hypothalamus and the hippocampus. Using stereotaxic injection of viral vectors in  
399 combination with transgenic mouse lines to express channelrhodopsin in a projection-specific  
400 manner, we have been able to selectively stimulate SuM axons in area CA2 of the  
401 hippocampus, allowing for the direct examination of synaptic transmission. This approach  
402 yielded novel functional physiological information about the SuM post-synaptic targets and  
403 overall consequences of activation. We found that, in contrast to previous anatomical reports,  
404 SuM inputs form synapses onto both PNs and INs in area CA2. The excitatory drive evoked  
405 by light-stimulation of SuM inputs was significantly larger for BC INs, which we demonstrate  
406 are likely PV+. The resulting feedforward inhibition recruited by SuM input stimulation  
407 enhanced the precision of AP timing of CA2 PNs in conditions of low and high cholinergic  
408 tone. The modified CA2 output evoked poly-synaptic inhibition in area CA1, likely  
409 responsible for a decrease firing rate of CA1 units in vivo. Overall, we demonstrate that SuM  
410 input controls CA2 output to area CA1 by recruiting feedforward inhibition.

### 411 SuM inputs to area CA2 form a microcircuit where PV+ basket cells strongly inhibit 412 pyramidal neurons

413 Glutamatergic innervation of area CA2 by the SuM has been previously described by tracing  
414 studies (Kiss et al., 2000; Soussi et al., 2010) and presumed to form synapses exclusively onto  
415 PNs (Maglóczy et al., 1994). Our experimental strategy allowed for the direct examination  
416 of the post-synaptic targets of SuM glutamatergic axons. Our results confirm that PNs in area  
417 CA2 indeed receive excitatory synapses from SuM axons. However, in contrast to what had  
418 been proposed in previous studies, we observed that SuM inputs target not only PNs but also  
419 INs in area CA2. Importantly, we identified a specific subpopulation of INs as PV+ BCs



420 which were the cell type most potently excited by SuM. These BCs could fire action  
421 potentials upon SuM inputs photostimulation leading to a substantial feedforward inhibition  
422 of neighboring PNs. Consistent with the perisomatic targeting of BCs axons, recruitment of  
423 BCs by SuM resulted in the control of PNs excitability. This finding demonstrates that SuM  
424 activity can pace action potential firing in PNs through recruitment of PV+ BCs. The  
425 inhibitory action of the SuM input to area CA2 contrasts with the overall excitatory effect of  
426 the SuM-DG path (Hashimoto et al., 2018; Li et al., 2020; Mizumori et al., 1989;  
427 Nakanishi et al., 2001).

#### 428 Consequences of SuM input on area CA2 output

429 Recent work has demonstrated a strong excitatory drive from area CA2 to CA1 (Chevalyere  
430 and Siegelbaum, 2010; Kohara et al., 2014; Nasrallah et al., 2019). Consequently,  
431 modification of CA2 output through synaptic plasticity (Nasrallah et al., 2019) or  
432 neuromodulation (Tirko et al., 2018) affects CA1 activity. This observation is critical when  
433 considering social memory formation, which is known to depend on CA2 output (Hitti and  
434 Siegelbaum, 2014; Stevenson and Caldwell, 2014) and is likely encoded in downstream  
435 ventral CA1 (Okuyama et al., 2016). CA2-targeting cells in the SuM have recently been  
436 shown to be highly active during novel social exploration (Chen et al., 2020). From our  
437 results, we hypothesize that this novel social signal from the SuM, acts via the PV+ inhibitory  
438 network in area CA2 to control the timing of CA2 output onto area CA1.

439 The population of INs potently excited by SuM transmission display many features that allow  
440 us to classify them as PV+ BCs. They have somas located in the somatic layer, have densely  
441 packed perisomatic-targeted axons, are fast spiking, show PV immuno-reactivity, are  
442 sensitive to MOR and DOR activation, and their selective silencing reduces SuM driven feed-  
443 forward inhibition of area CA2 PNs. Recent studies have indicated that DOR-mediated  
444 inhibitory synaptic plasticity of PV+ INs in area CA2 is required for social recognition  
445 memory (Domínguez et al., 2019) and further, that exposure to a novel conspecific induces a  
446 DOR-mediated plasticity in this same inhibitory network in area CA2 (Leroy et al., 2017)  
447 Thus, our finding that SuM input acts via PV+ interneurons fits with previous results, and  
448 provides a link between social novelty information and local hippocampal inhibitory  
449 plasticity.

450 By recruiting feedforward inhibition, SuM activity paces and temporally constrains AP firing  
451 from CA2 PNs undergoing depolarization. More critically, in conditions of elevated  
452 cholinergic tone relevant to SuM activity in vivo, CA2 PNs depolarize and fire bursts of APs



453 that can be shaped by SuM input both by controlling AP firing as well as membrane  
454 depolarization. While this result was obtained by triggering SuM input stimulation to the  
455 onset of burst firing by CA2 PNs, in vivo and acute slice experiments revealed a consistent  
456 influence of CA1 PN AP firing by SuM input to area CA2 regardless of the timing of SuM  
457 input stimulation relative to CA2 PN AP burst firing. These results demonstrate a powerful  
458 control of SuM input over CA2 output when PNs are spontaneously firing bursts of APs, a  
459 firing mode that is most efficient at influencing CA1 activity (Tirko et al., 2018). Optogenetic  
460 experiments have recently shown that CA2 PNs can drive a strong feedforward inhibition in  
461 area CA1 (Nasrallah et al., 2019). Although SuM input likely does not directly drive  
462 feedforward inhibition in area CA1 (Chen et al., 2020), the recruitment of feedforward  
463 inhibition in area CA2 by SuM input activation could curtail the time window of spontaneous  
464 firing in CA2 PNs and effectively lead to a synchronized drive of feedforward inhibition by  
465 area CA2 over area CA1. We postulate that the concerted IPSC that we detect in area CA1  
466 with SuM fiber photostimulation in area CA2 corresponds to the large decrease in firing that  
467 is observed in CA1 multi-unit recordings in vivo. Thus, these data provide evidence for a  
468 long-range control of CA2 bursting activity and the consequences in downstream area CA1 in  
469 conditions of high cholinergic tone that accompanies theta oscillations in vivo during which  
470 SuM is active.

#### 471 Gating of area CA2 activity by PV+ INs and significance for pathologies

472 The density of PV+ INs in area CA2 is strikingly higher than in neighboring areas CA3 and  
473 CA1 (Botcher et al., 2014; Piskorowski and Chevaleyre, 2013). This population of INs has  
474 been shown to play a powerful role in controlling the activation of CA2 PNs by CA3 inputs  
475 (Nasrallah et al., 2015). We show in this study that long-range inputs from the SuM can  
476 strongly recruit PV+ BCs, which in turn inhibit PNs in this area. Hence, both intra-  
477 hippocampal inputs from CA3 and long-range inputs from the SuM converge onto PV+ INs to  
478 control CA2 PN excitability and output.

479 Postmortem studies have reported losses of PV+ INs in area CA2 in pathological contexts  
480 including bipolar disorder (Benes et al., 1998), Alzheimer's disease (Brady and Mufson,  
481 1997), and schizophrenia (Benes et al., 1998; Knable et al., 2004). Consistent with these  
482 reports, in a mouse model of the 22q11.2 deletion syndrome, we found a loss of PV staining  
483 and deficit of inhibitory transmission in area CA2 that were accompanied by impairments in  
484 social memory (Piskorowski et al., 2016). We postulate that the PV+ INs altered during  
485 pathological conditions may be the same population of PV+ BCs recruited by long-range

486 SuM inputs. Indeed, the DOR-mediated plasticity onto PV+INs is altered in the 22q11.2  
487 deletion syndrome, and we show here that the PV+ INs targeted by the SuM also express  
488 DOR. Thus, the loss of function of PV+ INs in area CA2 could disrupt proper long-range  
489 connection between the hippocampus and the hypothalamus and possibly contribute to some  
490 of the cognitive impairments observed in schizophrenia animal models. Further,  
491 pharmacological mouse models of schizophrenia have reported increased c-fos  
492 immunoreactivity in the SuM as well as memory impairments (Castañé et al., 2015).  
493 Although several alterations in these models of schizophrenia could lead to deficits of  
494 hippocampal-dependent behavior, abnormalities of the SuM projection onto area CA2 appear  
495 as a potential mechanism that warrants further investigation.

496

## 497 **Materials & Methods**

498 All procedures involving animals were performed in accordance with institutional regulations  
499 (French Ministry of Research and Education protocol #12406-2016040417305913). Animal  
500 sample sizes were estimated using power tests with standard deviations and ANOVA values  
501 from pilot experiments. A 15 % failure rate was assumed to account for stereotaxic injection  
502 errors and slice preparation complications. Every effort was made to reduce animal suffering.

503 Use of the Tg(Slc17ab-icre)10Ki mouse line: we used the Tg(Slc17ab-icre)10Ki mouse line  
504 that was previously generated (Borgius et al., 2010) and expresses the Cre recombinase under  
505 the control slc17a6 gene coding for the vesicular glutamate transporter isoform 2 (VGluT2).

506 Use of the csf2rb2-Cre mouse line: We used the csf2rb2-Cre mouse line that was recently  
507 generated (Chen et al., 2020) and expresses the Cre recombinase under control of the csf2rb2  
508 gene that shows selective expression in the SuM.

509 Use of the Pvalbtm1(cre)Arbr/J mouse line: we used the Pvalbtm1(cre)Arbr/J mouse line that  
510 was previously generated (Hippenmeyer et al., 2005) and expresses the Cre recombinase  
511 under the control Pvalbm gene coding for parvalbumin (PV).

512 Stereotaxic viral injection: Animals were anaesthetized with ketamine (100 mg/kg) and  
513 xylazine (7 mg/kg). The adeno-associated viruses AAV9.EF1a.DIO.hChR2(H134R).EYFP  
514 and AAV9.hSynapsin.EGFP.WPRE.bGH were used at  $3 \times 10^8$  vg, the  
515 AAV.Synapsin.DIO.hM4D(Gi).mCherry was used at  $3.6 \times 10^9$  vg and the  
516 AAV2/9.hSyn.hChR2(H134R).EYFP.WPRE.hGH was used at  $3.7 \times 10^{13}$  vg. The retrograde  
517 tracer CAV2-cre virus was used at  $2.5 \times 10^{12}$  vg. 500 nL of virus was unilaterally injected into

518 the brain of 4 week-old male wild type C57BL6, Tg(Slc17ab-icre)10Ki (VGluT2-Cre),  
519 csf2rb2-cre (SuM-Cre) or Pvalbtm1(cre)Arbr/J (PV-Cre) mice at 100 nL/min and the  
520 injection cannula was left at the injection site for 10 min following infusion. In the case of  
521 AAV.Synapsin.DIO.hM4D(Gi)-mcherry injection in PV-Cre mice, bilateral injections were  
522 performed in dorsal CA2. The loci of the injection sites were as follows: anterior–posterior  
523 relative to bregma: -2.8 mm for SuM, -1.6 mm for CA2; medial-lateral relative to midline: 0  
524 mm for SuM, 1.9 mm for CA2; dorsal-ventral relative to surface of the brain: 4.75 mm for  
525 SuM, 1.4 mm for CA2.

526 Electrophysiological recordings: Transverse hippocampal slices were prepared at least 3  
527 weeks after viral injection and whole-cell patch-clamp recordings were performed from PNs  
528 and INs across the hippocampal CA regions. In the case of PV-Cre mice injected with  
529 AAV.Synapsin.DIO.hM4D(Gi)-mcherry, slices were prepared 6 weeks after viral injection.  
530 Animals were deeply anaesthetized with ketamine (100 mg/kg) and xylazine (7 mg/kg), and  
531 perfused transcardially with a N-methyl-D-glucamin-based (NMDG) cutting solution  
532 containing the following (in mM): NMDG 93, KCl 2.5, NaH<sub>2</sub>PO<sub>4</sub> 1.25, NaHCO<sub>3</sub> 30, HEPES  
533 20, glucose 25, thiourea 2, Na-ascorbate 5, Na-pyruvate 3, CaCl<sub>2</sub> 0.5, MgCl<sub>2</sub> 10. Brains were  
534 then rapidly removed, hippocampi were dissected out and placed upright into an agar mold  
535 and cut into 400 µm thick transverse slices (Leica VT1200S) in the same cutting solution at 4  
536 °C. Slices were transferred to an immersed-type chamber and maintained in artificial cerebro-  
537 spinal fluid (ACSF) containing the following (in mM) : NaCl 125, KCl 2.5, NaH<sub>2</sub>PO<sub>4</sub> 1.25,  
538 NaHCO<sub>3</sub> 26, glucose 10, Na-pyruvate 2, CaCl<sub>2</sub> 2, MgCl<sub>2</sub> 1. Slices were incubated at 32°C for  
539 approximately 20 min then maintained at room temperature for at least 45 min prior to patch-  
540 clamp recordings performed with either potassium- or cesium-based intracellular solutions  
541 containing the following (in mM): K- or Cs-methyl sulfonate 135, KCl 5, EGTA-KOH 0.1,  
542 HEPES 10, NaCl 2, MgATP 5, Na<sub>2</sub>GTP 0.4, Na<sub>2</sub>-phosphocreatine 10 and biocytin (4  
543 mg/mL).

544 ChR2 was excited by 488 nm light delivered by a LED attached to the epifluorescence port of  
545 the microscope. Light stimulation trains consisted of 2-10 pulses, 0.5 ms long, delivered at  
546 10 Hz, repeated every 20 s for at least 20 sweeps. For the patch-clamp recordings in area CA1  
547 with stimulation of SuM axons in area CA2, 50 ms long light stimulation pulses were  
548 delivered every 10 seconds. We used a light intensity of 25 mW/mm<sup>2</sup> which was  
549 experimentally determined as the lowest irradiance allowing TTX-sensitive maximal  
550 responses in all cell types and conditions. Data were obtained using a Multiclamp 700B

551 amplifier, sampled at 10 kHz and digitized using a Digidata. The pClamp10 software was  
552 used for data acquisition. Series resistance were < 20 MOhm and were not compensated in  
553 voltage-clamp, bridge balance was applied in current-clamp. An experimentally determined  
554 liquid junction potential of approximately 9 mV was not corrected for. Pharmacological  
555 agents were added to ACSF at the following concentrations (in  $\mu\text{M}$ ): 10 NBQX and 50 D-  
556 APV to block AMPA and NMDA receptors, 1 SR95531 and 2 CGP55845A to block GABA<sub>A</sub>  
557 and GABA<sub>B</sub> receptors, 1 DAMGO to activate  $\mu$ -opioid receptors (MOR), 0.5 DPDPE to  
558 activate  $\delta$ -opioid receptors (DOR), 10 clozapine N-oxide (CNO) to activate hM4D(Gi)  
559 DREADDs, 10 CCh to activate cholinergic receptors, 0.2 tetrodotoxin (TTX) to prevent sodic  
560 action potential generation.

561 Surgery for *in vivo* recordings: All surgeries were performed in a stereotaxic frame  
562 (Narishige). Csf2rb2-cre male mice from 3 to 6 months of age were anaesthetized using  
563 500  $\mu\text{g}/\text{kg}$  Avertin. pAAV.DIO.hChR2(H134R).EYFP was injected into the SuM (-2.7 mm  
564 AP, +0.4 mm ML, -5.0 mm DV) using a 10  $\mu\text{L}$  Hamilton microsyringe (701LT, Hamilton)  
565 with a beveled 33 gauge needle (NF33BL, World Precision Instruments (WPI)). A  
566 microsyringe pump (UMP3, WPI) with controller (Micro4, WPI) were used to set the speed  
567 of the injection (100 nl/min). The needle was slowly lowered to the target site and remained  
568 in place for 5 min prior to start of the injection and the needle was removed 10 min after  
569 infusion was complete. Following virus injection, a custom-built screw-driven microdrive  
570 containing six independently adjustable nichrome tetrodes (14  $\mu\text{m}$  diameter), gold-plated to  
571 an impedance of 200 to 250 k $\Omega$  was implanted, with a subset of tetrodes targeting CA1, and  
572 an optic fiber (200  $\mu\text{m}$  core diameter, NA=0.22) targeting CA2 (-1.9 mm AP, +/- 2.2 mm  
573 ML, -1.6 mm DV). Following recovery, the tetrodes were slowly lowered over several days  
574 to CA1 pyramidal cell layer, identified by characteristic local field potential patterns (theta  
575 and sharp-wave ripples) and high amplitude multiunit activity. During the adjustment period  
576 the animal was habituated every day to a small box in which recording and stimulation were  
577 performed.

578 *In vivo* recording protocol: Recording was commenced following tetrodes reaching CA1. To  
579 examine the impact of SuM terminal stimulation in CA2 the mice were returned to the small  
580 familiar box and trains of 10 light pulses (473 nm, 10 mW/mm<sup>2</sup> and pulse width 50 ms) were  
581 delivered to the CA2 at 10 Hz. The pulse train was repeated every 10 seconds for at least 20  
582 times as the animals freely explored the box. Multiunit activity was recorded using a  
583 DigitalLynx 4SX recording system running Cheetah v.5.6.0 acquisition software (Neuralynx).

584 Broadband signals from each tetrode were filtered between 600 and 6,000 Hz and recorded  
585 continuously at 32 kHz. Recording sites were later verified histologically with electrolytic  
586 lesions as described above and the position of the optic fiber was also verified from the track.

587 *In Vivo* data analysis:

588 Spike and event timestamps corresponding to onset of each laser pulse were imported into  
589 Matlab (MathWorks) and spikes which occurred 50 ms before and 100 ms after each laser  
590 pulse were extracted. Raster plots were generated using a 1 ms bin size. Similar results were  
591 obtained using 5 ms and 10 ms bin size (data not shown). Firing rate histograms were  
592 calculated by dividing total number of spikes in each time bin by that bin's duration. Each  
593 firing rate histogram was normalized by converting it into z-score values. Mean standard  
594 deviation values for the z-score calculation were taken from pre-laser pulse time period. To  
595 average the response across all mice, for each tetrode the firing rate in each bin was  
596 normalized to the average rate in the pre-laser period.

597 Immunocytochemistry and cell identification: Midbrains containing the injection site were  
598 examined post-hoc to ensure that infection was restricted to the SuM.

599 Post-hoc reconstruction of neuronal morphology and SuM axonal projections were performed  
600 on slices and midbrain tissue following overnight incubation in 4 % paraformaldehyde in  
601 phosphate buffered saline (PBS). Midbrain sections were re-sliced sagittally to 100  $\mu$ m thick  
602 sections. Slices were permeabilized with 0.2 % triton in PBS and blocked overnight with 3 %  
603 goat serum in PBS with 0.2 % triton. Primary antibody (life technologies) incubation was  
604 carried out in 3 % goat serum in PBS overnight at 4°C. Channelrhodopsin-2 was detected by  
605 chicken primary antibody to GFP (Life technologies) (1:10,000 dilution) and a alexa488-  
606 conjugated goat-anti chick secondary. Other primary antibodies used were mouse anti-RGS14  
607 (Neuromab) (1:300 dilution), rabbit anti- PCP4 (Sigma) (1:600 dilution), guinea pig anti-  
608 vGlut2 antibody (Milipore) (1:10,000 dilution), rabbit anti-parvalbumin antibody (Swant)  
609 (dilution 1:2000). Alexa-546-conjugated streptavidin (life technologies), secondary antibodies  
610 and far-red neurotrace (life technologies) incubations were carried out in block solution for 4  
611 hours at room temperature. Images were collected with a Zeiss 710 laser-scanning confocal  
612 microscope.

613 Reconstructed neurons were classified as either PNs or INs based on the extension and  
614 localization of their dendrites and axons. CA1, CA2 and CA3 PNs were identified based on  
615 their somatic localization, dendritic arborization and presence of thorny excrescences (TE).

616 Among INs with somas located in the pyramidal layer (stratum pyramidale, SP),  
617 discrimination between BCs and non-BCs was achieved based on the restriction of their axons  
618 to SP or not, respectively. When available, firing patterns upon injection of depolarizing  
619 current step injection, action potential (AP) half-width, amount of repolarizing sag current  
620 upon hyperpolarization from -70 mV to -100 mV by current step injection, membrane  
621 resistance ( $R_M$ ) and capacitance ( $C_M$ ) were additionally used for cell identification. CA2 and  
622 CA3a PNs displayed similar firing patterns, AP width, sag current,  $R_M$  and  $C_M$ . In contrast,  
623 INs had faster firing rates, shorter AP width, higher  $R_M$  and lower  $C_M$  than PNs. BCs further  
624 differed from non-BCs by the presence of a larger sag current. All recorded neurons that  
625 could not be unequivocally identified as PNs or INs were excluded from analysis.

626 Data analysis and statistics: Electrophysiological recordings were analyzed using IGORpro  
627 (Wavemetrics) and Clampfit (Molecular devices) software. For accurate measurements of the  
628 kinetics and latencies of post-synaptic responses, the following detection process was used.  
629 For each cell, average traces were used to create a template waveform that was then fitted to  
630 individual traces and measurements were performed on the fitted trace. When only amplitudes  
631 of responses were needed, standard average peak detection was used. Results are reported  $\pm$   
632 SEM. Statistical significance was assessed using  $\chi^2$  test, Student's T test, Mann-Whitney U  
633 test, Wilcoxon signed-rank test, Kolmogorov-Smirnoff test, Kruskal-Wallis test, one-way or  
634 two-way ANOVA where appropriate.

635

### 636 **Author Contributions**

637 RAP, VR & TM designed experiments. RAP, VR, VC, LT, RB, AJYH performed  
638 experiments. VR, RAP and DP completed analysis. VR and RAP wrote the manuscript with  
639 input from all authors.

640

### 641 **Acknowledgments**

642 This work was supported by the RIKEN Center for Brain Science (TJM), Grant-in-Aid for  
643 Scientific Research from MEXT (19H05646; T.J.M), Grant-in-Aid for Scientific Research on  
644 Innovative Areas from MEXT (19H05233; T.J.M), ANR-13-JSV4-0002-01 (RAP), ANR-18-  
645 CE37-0020-01 (RAP), the Ville de Paris Programme Emergences (RAP), and the Brain and  
646 Behavioral Research Foundation NARSAD Young Investigator Grant (RAP) and the  
647 Foundation Recherche Médicale, FRM:FTD20170437387 (VR).



648

## 649 **References**

- 650 Aranda, L., Santín, L.J., Begega, A., Aguirre, J.A., and Arias, J.L. (2006). Supramammillary  
651 and adjacent nuclei lesions impair spatial working memory and induce anxiolytic-like  
652 behavior. *Behav Brain Res* *167*, 156–164.
- 653 Aranda, L., Begega, A., Sánchez-López, J., Aguirre, J.A., Arias, J.L., and Santín, L.J. (2008).  
654 Temporary inactivation of the supramammillary area impairs spatial working memory and  
655 spatial reference memory retrieval. *Physiology Behav* *94*, 322–330.
- 656 Bartesaghi, R., and Ravasi, L. (1999). Pyramidal neuron types in field CA2 of the guinea pig.  
657 *Brain Research Bulletin* *50*, 263–273.
- 658 Benes, F.M., Kwok, E.W., Vincent, S.L., and Todtenkopf, M.S. (1998). A reduction of  
659 nonpyramidal cells in sector CA2 of schizophrenics and manic depressives. *Biol Psychiat* *44*,  
660 88–97.
- 661 Berger, B., Esclapez, M., Alvarez, C., Meyer, G., and Catala, M. (2001). Human and monkey  
662 fetal brain development of the supramammillary-hippocampal projections: A system involved  
663 in the regulation of theta activity. *J Comp Neurol* *429*, 515–529.
- 664 Boehringer, R., Polygalov, D., Huang, A.J.Y., Middleton, S.J., Robert, V., Wintzer, M.E.,  
665 Piskorowski, R.A., Chevaleyre, V., and McHugh, T.J. (2017). Chronic Loss of CA2  
666 Transmission Leads to Hippocampal Hyperexcitability. *Neuron* *94*, 642-655.e9.
- 667 Borgius, L., Restrepo, C.E., Leao, R.N., Saleh, N., and Kiehn, O. (2010). A transgenic mouse  
668 line for molecular genetic analysis of excitatory glutamatergic neurons. *Mol Cell Neurosci* *45*,  
669 245–257.
- 670 Borhegyi, Z., Maglóczy, Z., Acsády, L., and Freund, T.F. (1998). The supramammillary  
671 nucleus innervates cholinergic and GABAergic neurons in the medial septum-diagonal band  
672 of Broca complex. *Neuroscience* *82*, 1053–1065.
- 673 Botcher, N.A., Falck, J.E., Thomson, A.M., and Mercer, A. (2014). Distribution of  
674 interneurons in the CA2 region of the rat hippocampus. *Frontiers Neuroanatomy* *8*, 104.
- 675 Boulland, J.-L., Jenstad, M., Boekel, A.J., Wouterlood, F.G., Edwards, R.H., Storm-Mathisen,  
676 J., and Chaudhry, F.A. (2009). Vesicular glutamate and GABA transporters sort to distinct  
677 sets of vesicles in a population of presynaptic terminals. *Cereb Cortex* *19*, 241–248.
- 678 Brady, D.R., and Mufson, E.J. (1997). Parvalbumin-immunoreactive neurons in the  
679 hippocampal formation of Alzheimer’s diseased brain. *Neuroscience* *80*, 1113–1125.
- 680 Buzsáki, G., and Moser, E.I. (2013). Memory, navigation and theta rhythm in the  
681 hippocampal-entorhinal system. *Nat Neurosci* *16*, 130–138.



- 682 Castañé, A., Santana, N., and Artigas, F. (2015). PCP-based mice models of schizophrenia:  
683 differential behavioral, neurochemical and cellular effects of acute and subchronic treatments.  
684 *Psychopharmacology* 232, 4085–4097.
- 685 Cembrowski, M.S., Wang, L., Sugino, K., Shields, B.C., Spruston, N., and Marder, E. (2016).  
686 Hipposeq: a comprehensive RNA-seq database of gene expression in hippocampal principal  
687 neurons. *Elife* 5, e14997.
- 688 Chen, S., He L., Huang, A.J.Y., Boehringer, R., Robert, V., Wintzer, M.E., Polygalov, D.,  
689 Weitemier, A.Z., Tao, Y., Gu, M., Middleton, S.J, Namiki, K., Hama, H., Therreau, L.,  
690 Chevaleyre, V., Hioki, H., Miyawaki, A., Piskorowski, R.A., McHugh, T.J. (2020). A  
691 hypothalamic novelty signal modulates hippocampal memory. *Nature*, *in press*. (*Will be*  
692 *published online September 30<sup>th</sup>, 2020, and in print October 8th, 2020*).
- 693 Chevaleyre, V., and Siegelbaum, S.A. (2010). Strong CA2 pyramidal neuron synapses define  
694 a powerful disinaptic cortico-hippocampal loop. *Neuron* 66, 560–572.
- 695 Dasgupta, A., Lim, Y.J., Kumar, K., Baby, N., Pang, K.L.K., Benoy, A., Behnisch, T., and  
696 Sajikumar, S. (2020). Group III metabotropic glutamate receptors gate long-term potentiation  
697 and synaptic tagging/capture in rat hippocampal area CA2. *ELife* 9, 919–920.
- 698 Domínguez, S., Rey, C.C., Therreau, L., Fanton, A., Massotte, D., Verret, L., Piskorowski,  
699 R.A., and Chevaleyre, V. (2019). Maturation of PNN and ErbB4 Signaling in Area CA2  
700 during Adolescence Underlies the Emergence of PV Interneuron Plasticity and Social  
701 Memory. *CellReports* 29, 1099-1112.e4.
- 702 Eichenbaum, H., and Cohen, N.J. (2014). Can we reconcile the declarative memory and  
703 spatial navigation views on hippocampal function? *Neuron* 83, 764–770.
- 704 Glickfeld, L.L., Atallah, B.V., and Scanziani, M. (2008). Complementary modulation of  
705 somatic inhibition by opioids and cannabinoids. *J Neurosci* 28, 1824–1832.
- 706 Gutiérrez-Guzmán, B.E., Hernández-Pérez, J.J., López-Vázquez, M.Á., Fregozo, C.S.,  
707 Guevara, M.Á., and Olvera-Cortés, M.E. (2012). Serotonin depletion of  
708 supramammillary/posterior hypothalamus nuclei produces place learning deficiencies and  
709 alters the concomitant hippocampal theta activity in rats. *Eur J Pharmacol* 682, 99–109.
- 710 Haglund, L., Swanson, L.W., and Köhler, C. (1984). The projection of the supramammillary  
711 nucleus to the hippocampal formation: an immunohistochemical and anterograde transport  
712 study with the lectin PHA-L in the rat. *J Comp Neurol* 229, 171–185.
- 713 Halasy, K., Hajszan, T., Kovács, E.G., Lam, T.-T., and Leranth, C. (2004). Distribution and  
714 origin of vesicular glutamate transporter 2-immunoreactive fibers in the rat hippocampus.  
715 *Hippocampus* 14, 908–918.
- 716 Hashimoto-dani, Y., Karube, F., Yanagawa, Y., Fujiyama, F., and Kano, M. (2018).  
717 Supramammillary Nucleus Afferents to the Dentate Gyrus Co-release Glutamate and GABA  
718 and Potentiate Granule Cell Output. *Cell Reports* 25, 2704-2715.e4.

- 719 Hernández-Pérez, J.J., Gutiérrez-Guzmán, B.E., López-Vázquez, M.Á., and Olvera-Cortés,  
720 M.E. (2015). Supramammillary serotonin reduction alters place learning and concomitant  
721 hippocampal, septal, and supramammillary theta activity in a Morris water maze. *Frontiers*  
722 *Pharmacol* 6, 250.
- 723 Hippenmeyer, S., Vrieseling, E., Sigrist, M., Portmann, T., Laengle, C., Ladle, D.R., and  
724 Arber, S. (2005). A Developmental Switch in the Response of DRG Neurons to ETS  
725 Transcription Factor Signaling. *Plos Biol* 3, e159.
- 726 Hitti, F.L., and Siegelbaum, S.A. (2014). The hippocampal CA2 region is essential for social  
727 memory. *Nature* 508, 88–92.
- 728 Ikemoto, S. (2005). The supramammillary nucleus mediates primary reinforcement via  
729 GABA(A) receptors. *Neuropsychopharmacol* 30, 1088–1095.
- 730 Ikemoto, S., Witkin, B.M., Zangen, A., and Wise, R.A. (2004). Rewarding effects of AMPA  
731 administration into the supramammillary or posterior hypothalamic nuclei but not the ventral  
732 tegmental area. *J Neurosci* 24, 5758–5765.
- 733 Ito, H.T., Moser, E.I., and Moser, M.-B. (2018). Supramammillary Nucleus Modulates Spike-  
734 Time Coordination in the Prefrontal-Thalamo- Hippocampal Circuit during Navigation.  
735 *Neuron* 99, 576-587.e5.
- 736 Ito, M., Shirao, T., Doya, K., and Sekino, Y. (2009). Three-dimensional distribution of Fos-  
737 positive neurons in the supramammillary nucleus of the rat exposed to novel environment.  
738 *Neurosci Res* 64, 397–402.
- 739 Kay, K., Sosa, M., Chung, J.E., Karlsson, M.P., Larkin, M.C., and Frank, L.M. (2016). A  
740 hippocampal network for spatial coding during immobility and sleep. *Nature* 531, 185–190.
- 741 Kiss, J., Csáki, Á., Bokor, H., Shanabrough, M., and Leranth, C. (2000). The supramammillo-  
742 hippocampal and supramammillo-septal glutamatergic/aspartatergic projections in the rat: a  
743 combined [3H]d-aspartate autoradiographic and immunohistochemical study. *Neuroscience*  
744 97, 657–669.
- 745 Klausberger, T., and Somogyi, P. (2008). Neuronal diversity and temporal dynamics: the  
746 unity of hippocampal circuit operations. *Science* 321, 53–57.
- 747 Knable, M.B., Barci, B.M., Webster, M.J., Meador-Woodruff, J., Torrey, E.F., and  
748 Consortium, S.N. (2004). Molecular abnormalities of the hippocampus in severe psychiatric  
749 illness: postmortem findings from the Stanley Neuropathology Consortium. *Mol Psychiatr* 9,  
750 609-20–544.
- 751 Kocsis, B., and Vertes, R.P. (1994). Characterization of neurons of the supramammillary  
752 nucleus and mammillary body that discharge rhythmically with the hippocampal theta rhythm  
753 in the rat. *J Neurosci* 14, 7040–7052.
- 754 Kohara, K., Pignatelli, M., Rivest, A.J., Jung, H.-Y., Kitamura, T., Suh, J., Frank, D.,  
755 Kajikawa, K., Mise, N., Obata, Y., et al. (2014). Cell type-specific genetic and optogenetic  
756 tools reveal hippocampal CA2 circuits. *Nat Neurosci* 17, 269–279.

- 757 Lein, E.S., Zhao, X., and Gage, F.H. (2004). Defining a Molecular Atlas of the Hippocampus  
758 Using DNA Microarrays and High-Throughput In Situ Hybridization. *Journal of*  
759 *Neuroscience* 24, 3879–3889.
- 760 Leroy, F., Brann, D.H., Meira, T., and Siegelbaum, S.A. (2017). Input-Timing-Dependent  
761 Plasticity in the Hippocampal CA2 Region and Its Potential Role in Social Memory. *Neuron*  
762 95, 1089-1102.e5.
- 763 Li, Y., Bao, H., Luo, Y., Yoan, C., Sullivan, H.A., Quintanilla, L., Wickersham, I., Lazarus,  
764 M., Shin, Y.-Y.I., and Song, J. (2020). Supramammillary nucleus synchronizes with dentate  
765 gyrus to regulate spatial memory retrieval through glutamate release. *ELife* 9, 604–623.
- 766 Maglóczy, Z., Acsády, L., and Freund, T.F. (1994). Principal cells are the postsynaptic  
767 targets of supramammillary afferents in the hippocampus of the rat. *Hippocampus* 4, 322–  
768 334.
- 769 May, M.V.L., Hume, C., Sabatier, N., Schéle, E., Bake, T., Bergström, U., Menzies, J., and  
770 Dickson, S.L. (2019). Activation of the rat hypothalamic supramammillary nucleus by food  
771 anticipation, food restriction or ghrelin administration. *Journal of Neuroendocrinology* 31,  
772 e12676-14.
- 773 Mizumori, S.J., McNaughton, B.L., and Barnes, C.A. (1989). A comparison of  
774 supramammillary and medial septal influences on hippocampal field potentials and single-unit  
775 activity. *Journal of Neurophysiology* 61, 15–31.
- 776 Nakanishi, K., Saito, H., and Abe, K. (2001). The supramammillary nucleus contributes to  
777 associative EPSP-spike potentiation in the rat dentate gyrus in vivo. *Eur J Neurosci* 13, 793–  
778 800.
- 779 Nasrallah, K., Piskorowski, R.A., and Chevaleyre, V. (2015). Inhibitory Plasticity Permits the  
780 Recruitment of CA2 Pyramidal Neurons by CA3(1,2,3). *Eneuro* 2, 1–12.
- 781 Nasrallah, K., Therreau, L., Robert, V., Huang, A.J.Y., McHugh, T.J., Piskorowski, R.A., and  
782 Chevaleyre, V. (2019). Routing Hippocampal Information Flow through Parvalbumin  
783 Interneuron Plasticity in Area CA2. *Cell Reports* 27, 86-98.e3.
- 784 No, R.L. de (1934). Studies on the Structure of the Cerebral Cortex. II. Continuation of the  
785 Study of the Ammonic System. *Journal f. Psychologie and Neurologie* 113–175.
- 786 Okuyama, T., Kitamura, T., Roy, D.S., Itohara, S., and Tonegawa, S. (2016). Ventral CA1  
787 neurons store social memory. *Science* 353, 1536–1541.
- 788 Oliva, A., Fernández-Ruiz, A., Buzsáki, G., and Berényi, A. (2016). Role of Hippocampal  
789 CA2 Region in Triggering Sharp-Wave Ripples. *Neuron* 91, 1342–1355.
- 790 Pan, W., and McNaughton, N. (2002). The role of the medial supramammillary nucleus in the  
791 control of hippocampal theta activity and behaviour in rats. *Eur J Neurosci* 16, 1797–1809.
- 792 Pan, W.-X., and McNaughton, N. (1997). The medial supramammillary nucleus, spatial  
793 learning and the frequency of hippocampal theta activity. *Brain Res* 764, 101–108.

- 794 Pan, W.-X., and McNaughton, N. (2004). The supramammillary area: its organization,  
795 functions and relationship to the hippocampus. *Prog Neurobiol* 74, 127–166.
- 796 Pawelzik, H., Hughes, D.I., and Thomson, A.M. (2002). Physiological and morphological  
797 diversity of immunocytochemically defined parvalbumin- and cholecystokinin-positive  
798 interneurons in CA1 of the adult rat hippocampus. *J Comp Neurol* 443, 346–367.
- 799 Pedersen, N.P., Ferrari, L., Venner, A., Wang, J.L., Abbott, S.B.G., Vujovic, N., Arrigoni, E.,  
800 Saper, C.B., and Fuller, P.M. (2017). Supramammillary glutamate neurons are a key node of  
801 the arousal system. *Nat Commun* 8, 1–16.
- 802 Piskorowski, R.A., and Chevalyere, V. (2013). Delta-opioid receptors mediate unique  
803 plasticity onto parvalbumin-expressing interneurons in area CA2 of the hippocampus. *J*  
804 *Neurosci* 33, 14567–14578.
- 805 Piskorowski, R.A., Nasrallah, K., Diamantopoulou, A., Mukai, J., Hassan, S.I., Siegelbaum,  
806 S.A., Gogos, J.A., and Chevalyere, V. (2016). Age-Dependent Specific Changes in Area CA2  
807 of the Hippocampus and Social Memory Deficit in a Mouse Model of the 22q11.2 Deletion  
808 Syndrome. *Neuron* 89, 163–176.
- 809 Plaisier, F., Hume, C., and Menzies, J. (2020). Neural connectivity between the hypothalamic  
810 supramammillary nucleus and appetite- and motivation-related regions of the rat brain.  
811 *Journal of Neuroendocrinology* jne.12829-31.
- 812 Renouard, L., Billwiller, F., Ogawa, K., Clément, O., Camargo, N., Abdelkarim, M., Gay, N.,  
813 Scoté-Blachon, C., Touré, R., Libourel, P.-A., et al. (2015). The supramammillary nucleus  
814 and the claustrum activate the cortex during REM sleep. *Sci Adv* 1, e1400177–e1400177.
- 815 Robert, V., Therreau, L., Davatolhagh, M.F., Bernardo-Garcia, F.J., Clements, K.N.,  
816 Chevalyere, V., and Piskorowski, R.A. (2020). The mechanisms shaping CA2 pyramidal  
817 neuron action potential bursting induced by muscarinic acetylcholine receptor activation. *J*  
818 *Gen Physiol* 152.
- 819 Shahidi, S., Motamedi, F., and Naghdi, N. (2004). Effect of reversible inactivation of the  
820 supramammillary nucleus on spatial learning and memory in rats. *Brain Res* 1026, 267–274.
- 821 Soussi, R., Zhang, N., Tahtakran, S., Houser, C.R., and Esclapez, M. (2010). Heterogeneity of  
822 the supramammillary-hippocampal pathways: evidence for a unique GABAergic  
823 neurotransmitter phenotype and regional differences. *Eur J Neurosci* 32, 771–785.
- 824 Srinivas, K.V., Buss, E.W., Sun, Q., Santoro, B., Takahashi, H., Nicholson, D.A., and  
825 Siegelbaum, S.A. (2017). The Dendrites of CA2 and CA1 Pyramidal Neurons Differentially  
826 Regulate Information Flow in the Cortico-Hippocampal Circuit. *J Neurosci* 37, 3276–3293.
- 827 Stagkourakis, S., Spigolon, G., Williams, P., Protzmann, J., Fisone, G., and Broberger, C.  
828 (2018). A neural network for intermale aggression to establish social hierarchy. *Nat Neurosci*  
829 21, 834–842.
- 830 Stevenson, E.L., and Caldwell, H.K. (2014). Lesions to the CA2 region of the hippocampus  
831 impair social memory in mice. *Eur J Neurosci* 40.

- 832 Sun, Q., Srinivas, K.V., Sotayo, A., and Siegelbaum, S.A. (2014). Dendritic Na(+) spikes  
833 enable cortical input to drive action potential output from hippocampal CA2 pyramidal  
834 neurons. *Elife* 3, 7750.
- 835 Tirko, N.N., Eyring, K.W., Carcea, I., Mitre, M., Chao, M.V., Froemke, R.C., and Tsien,  
836 R.W. (2018). Oxytocin Transforms Firing Mode of CA2 Hippocampal Neurons. *Neuron* 100,  
837 593-608.e3.
- 838 Vertes, R.P. (1992). PHA-L analysis of projections from the supramammillary nucleus in the  
839 rat. *J Comp Neurol* 326, 595–622.
- 840 Vertes, R.P., and Kocsis, B. (1997). Brainstem-diencephalo-septohippocampal systems  
841 controlling the theta rhythm of the hippocampus. *Neuroscience* 81, 893–926.
- 842 Vicente, A.F., Slézia, A., Ghestem, A., Bernard, C., and Quilichini, P.P. (2020). In Vivo  
843 Characterization of Neurophysiological Diversity in the Lateral Supramammillary Nucleus  
844 during Hippocampal Sharp-wave Ripples of Adult Rats. *Neuroscience* 435, 95–111.
- 845 Wyss, J.M., Swanson, L.W., and Cowan, W.M. (1979). Evidence for an input to the  
846 molecular layer and the stratum granulosum of the dentate gyrus from the supramammillary  
847 region of the hypothalamus. *Anat Embryol* 156, 165–176.
- 848 Zhao, M., Choi, Y.-S., Obrietan, K., and Dudek, S.M. (2007). Synaptic plasticity (and the lack  
849 thereof) in hippocampal CA2 neurons. *J Neurosci* 27, 12025–12032.

850

851

## 852 **Figures legends**

853 **Figure 1. Selective functional mapping of SuM neurons that project to hippocampal**  
854 **area CA2.** A. Left, diagram illustrating the injection of AAVs into the SuM. Middle, sagittal  
855 image indicating the infected SuM area expressing hCHR2(H134R)-EYFP (green). Right,  
856 expanded view of injection site in the Csf2rbr-Cre mouse line. B. Left, hCHR2(H134R)-  
857 EYFP -expressing SuM fibers (green) and nissl staining (blue) in the hippocampus. Right,  
858 higher magnification image of area CA2 with hCHR2(H134R)-EYFP -expressing SuM fibers  
859 (green) and nissl staining (blue) and RGS14 staining (magenta) to label area CA2. C. CA2  
860 pyramidal neurons in the SuM-innervated region receive excitatory transmission. (C1)  
861 Example CA2 PN reconstruction (dendrites in black, axons in grey, hippocampal stratum  
862 borders shown in dotted line, area demarcated in blue corresponds to the expanded image in  
863 C2). (C2) Biocytin labeling of the recorded cell proximal dendrites, scale bar represents 10  
864  $\mu\text{m}$ . (C3) AP firing and repolarizing sag current in response to steps of +800 and -400 pA  
865 current injection. (C4) Light-evoked EPSPs (top traces, individual traces shown in grey,

866 average trace shown in black) and EPSCs (bottom traces, individual traces shown in grey,  
867 average trace shown in black). **D.** CA3 pyramidal neurons in the SuM-innervated region  
868 receive excitatory transmission. (D1) Example CA3 PN reconstruction (dendrites in brown,  
869 axons in light brown, hippocampal stratum borders shown in dotted line, area demarcated in  
870 blue corresponds to the expanded image in D2). (D2) Biocytin labeling of the recorded cell  
871 proximal dendrites, note the presence of thorny excrescences, as indicated by the red arrows;  
872 scale bar represents 10  $\mu$ m. (D3) AP firing and repolarizing sag current in response to steps of  
873 +800 and -400 pA current injection. (D4) Light-evoked EPSPs (top traces, individual traces  
874 shown in grey, average trace shown in black) and EPSCs (bottom traces, individual traces  
875 shown in grey, average trace shown in black). **E.** Diagram illustrating the whole-cell  
876 recordings of area CA2 PNs and SuM fiber light stimulation in acute slice preparation. **F.**  
877 Sample traces of three 10 Hz SuM light-evoked PSPs before and after blocking inhibitory  
878 transmission (control shown in black, SR95531 & CGP55845A shown in grey). **G.** Summary  
879 graph of light-evoked PSP amplitudes recorded in PNs before and after application of 1  $\mu$ M  
880 SR95531 & 2  $\mu$ M CGP55845A (individual cells shown as thin lines, population average  
881 shown as thick line, error bars represent SEM,  $n = 14$ ; Wilcoxon signed-rank tests,  $p = 0.004$   
882 for the first PSP,  $p = 0.013$  for the second PSP,  $p < 0.001$  for the third PSP).

883

884 **Figure 2. SuM input provides excitatory glutamatergic transmission to diverse**  
885 **population of PNs in area CA2.** A-B. Left, diagrams illustrating whole-cell recordings in  
886 area CA2 and SuM fiber stimulation in acute slice preparation. Middle, example  
887 reconstruction of different cell types (soma and dendrites in thick lines, axon in thin lines,  
888 hippocampal strata in dotted grey lines). Right, sample traces of light-evoked EPSPs (top,  
889 individual traces in grey, average trace in black) and EPSCs (bottom, individual traces in  
890 grey, average trace in black). **A.** A Basket cell in area CA2. **B.** Non-basket cell. **C.** Summary  
891 graph of light-evoked EPSC potencies in PNs, BCs and non-BCs in area CA2 (individual  
892 cells shown as dots, population average shown as thick line, error bars represent SEM, PNs :  
893  $n = 166$ ; BC INs:  $n = 18$ ; non-BCs:  $n = 13$ ; Kruskal-Wallis test with Dunn-Holland-Wolfe  
894 post hoc test,  $p = 0.022$ ). **D.** Summary graph of light-evoked PSP amplitudes in PNs, BCs and  
895 non-BCs (individual cells shown as dots, population average shown as thick line, error bars  
896 represent SEM, PNs :  $n = 20$ ; BCs :  $n = 10$ ; non-BCs :  $n = 4$ ; Kruskal-Wallis test with Dunn-  
897 Holland-Wolfe post hoc test,  $p < 0.001$ ). **E.** Left, proportion of post-synaptic CA2 PNs, BCs  
898 and non-BCs firing action potentials time-locked to light stimulation of SuM input. Right,



899 sample traces of light-evoked action potentials in a BC recorded in current-clamp at resting  
900 membrane potential (top) and in cell-attached (bottom) configurations.

901

902 **Figure 3. SuM inputs provide excitation to Parvalbumin-expressing BCs.** A. Three  
903 biocytin reconstructions of BC INs with dendrites in red and axons in light red. Inset, current  
904 clamp steps to -400 pA and +400 pA display high-frequency AP firing and repolarizing sag  
905 current. B. Corresponding light-evoked EPSCs and EPSPs for the three reconstructed neurons  
906 (individual traces in grey, average trace in black). C. Corresponding PV immunostaining of  
907 the three interneurons: parvalbumin staining, biocytin labeling of the recorded cell, and merge  
908 (PV in magenta and biocytin in green).

909

910 **Figure 4. Parvalbumin-expressing BCs mediate the feedforward inhibition recruited by**  
911 **photostimulation of SuM fibers.** A. Application of the mu-opioid receptor agonist,  
912 DAMGO, results in the complete abolition of light-evoked SuM inhibitory transmission. A1,  
913 sample traces (top, control in red, DAMGO in grey) and summary graph of light-evoked IPSC  
914 amplitudes recorded in area CA2 PNs before and after application of 1  $\mu$ M DAMGO (bottom,  
915 n = 6, error bars represent SEM). A2, sample traces (top, SR95531 & CGP55845A in black,  
916 DAMGO in grey) and summary graph of light-evoked EPSC amplitudes recorded in area  
917 CA2 PNs before and after application of 1 $\mu$ M DAMGO (bottom, n = 17, error bars represent  
918 SEM). B. Application of the delta-opioid receptor agonist, DPDPE, results in the long-term  
919 depression of light-evoked SuM inhibitory transmission. B1, sample traces (top, control in  
920 red, DPDPE in grey) and summary graph of light-evoked IPSC amplitudes recorded in area  
921 CA2 PNs before and after application of 0.5  $\mu$ M DPDPE (bottom, n = 7, error bars represent  
922 SEM). B2, sample traces (top, SR95531 & CGP55845A in black, DAMGO in grey) and  
923 summary graph of light-evoked EPSC amplitudes recorded in area CA2 PNs before and after  
924 application of 0.5  $\mu$ M DPDPE (bottom, n = 7, error bars represent SEM). C. Left, diagrams  
925 illustrating the method to infect SuM neurons and selectively inhibit PV+ INs in area CA2.  
926 An AAV allowing the Cre-dependent expression of inhibitory DREADD was injected  
927 bilaterally into area CA2 of the dorsal hippocampus and another AAV allowing the  
928 expression of ChR2 was injected into the SuM of PV-Cre mice, allowing optogenetic  
929 stimulation of SuM inputs and pharmacogenetic inhibition of PV+ INs by application of the  
930 DREADD agonist CNO at 10  $\mu$ M. Right, diagram of the recording configuration. D.  
931 Silencing of PV+ INs by inhibitory DREADDs reduces SuM feedforward inhibition onto area



932 CA2 PNs. Sample traces (left, control in red, CNO in grey) and summary graph (right) of  
933 light-evoked IPSC amplitudes recorded in CA2 PNs before and after application of 10 $\mu$ M  
934 CNO (n = 13, error bars represent SEM). E. Example immunostaining against PV and  
935 DREADD with biocytin labelling in area CA2 from a slice used in these experiments.

936

937 **Figure 5. Area CA2 PNs receive a net inhibitory drive from SuM that controls AP firing**  
938 **properties.** A. Diagram illustrating whole-cell recordings of area CA2 PNs and SuM fiber  
939 light stimulation in acute slice preparation. B. Example traces of a CA2 PN action potential  
940 firing in response to current injection in the absence (black traces) or presence of 10 Hz  
941 photostimulation of SuM inputs (red traces). C. Action potential onset is increased with 10 Hz  
942 SuM input photostimulation. Left, sample traces of the first AP in control and with inhibition  
943 blocked by 1  $\mu$ M SR95531 & 2  $\mu$ M CGP55845A application (light-off in black, light-on in  
944 red, light-off in SR95531 & CGP55845A in grey, light-on in SR95531 & CGP55845A in  
945 purple). Right, summary graph of photostimulation-induced delay of AP firing in area CA2  
946 PNs before and after application of SR95531 & CGP55845A (control shown in red, n = 12,  
947 paired-T test, p = 0.016; SR95531 & CGP55845A shown in purple, n = 6; Wilcoxon signed-  
948 rank test, p = 0.44; individual cells shown with dots, boxplot represents median, quartiles, 10<sup>th</sup>  
949 and 90<sup>th</sup> percentiles). D. Sample traces of AP firing in repeated trials (light-off in black, light-  
950 on in red, light-on in SR95531 & CGP55845A in purple; during experiment photostimulation  
951 was interleaved with control, but are grouped here for demonstration purposes). E. AP jitter in  
952 CA2 PNs is reduced by activation of SuM inputs. Left, summary graph of the standard  
953 deviation of AP firing with or without 10 Hz photostimulation (n = 12; Wilcoxon signed-rank  
954 test, p < 0.001 for the first AP, p = 0.008 for the second AP, p = 0.004 for the third AP;  
955 individual cells shown with thin lines, population average shown as thick line, error bars  
956 represent SEM). Right, photostimulation-induced reduction of AP firing standard deviation in  
957 control and in SR95531 & CGP55845A (control, n = 12; Wilcoxon signed-rank tests, p <  
958 0.001 for the first AP, p = 0.008 for the second AP, p = 0.004 for the third AP; SR95531 &  
959 CGP55845A, n = 6; Wilcoxon signed-rank tests, p = 0.22 for the first AP, p = 0.16 for the  
960 second AP, p = 0.09 for the third AP; individual cells shown with dots, boxplot represents  
961 median, quartiles, 10<sup>th</sup> and 90<sup>th</sup> percentiles).

962

963 **Figure 6. SuM input shapes CA2 PN AP bursts in conditions of elevated cholinergic**  
964 **tone.** A. Diagram illustrating whole-cell recordings of area CA2 PNs with light stimulation of

965 SuM fibers in an acute slice preparation. B. Sample trace of spontaneous AP bursting activity  
966 recorded from a CA2 PN during bath application of 10  $\mu$ M CCh. For every even-numbered  
967 burst, a 10 Hz photostimulation (blue bars) was delivered to excite SuM inputs in area CA2  
968 allowing a comparison of burst AP firing in the same cell. C. Sample traces of AP firing  
969 during bursts for light-off (left, black) and light-on (right, red) epochs. D. Comparison of AP  
970 number / burst for light-off (black) and light-on (red) events ( $n = 7$ ; individual cells shown as  
971 thin lines, population average shown as thick line, error bars represent SEM; paired-T test,  $p =$   
972 0.031). E. Average firing rate during spontaneous burst events with SuM photostimulation  
973 (red, light-on) and controlled inter-leaved burst events (black, light-off). Shaded area  
974 represents SEM for 7 cells each with between 3 and 13 bursts analyzed in light-on and light-  
975 off conditions (2-way ANOVA, light factor:  $p < 0.001$ , time factor:  $p < 0.001$ , light x time  
976 factor:  $p = 0.052$ ). F. Example burst events with (red) and without (black) SuM  
977 photostimulation overlaid and on a scale that shows the rapidly hyperpolarizing membrane  
978 potential that occurs with SuM input stimulation. G. Comparison of bursts duration for events  
979 with (red) and without (black) photostimulation ( $n = 7$ ; individual cells shown as thin lines,  
980 population average shown as thick line, error bars represent SEM; paired-T test,  $p = 0.037$ ).  
981 H. Comparison of time elapsed to next burst onset following bursts with (red) or without  
982 (black) photostimulation ( $n = 7$ ; individual cells shown as thin lines, population average shown  
983 as thick line, error bars represent SEM; paired-T test,  $p = 0.001$ ).

984 **Figure 7. Consequences of SuM input on area CA2 output to CA1.** A. Diagram  
985 illustrating in vivo recording in CA1 with tetrodes and SuM axon terminals stimulation over  
986 CA2 with an implanted optical fiber. B. Representative data from 4 multi-unit recordings.  
987 Raster plot (top) showing CA1 AP firing activity before and during photostimulation of SuM  
988 fibers in area CA2. The corresponding firing rate histogram (middle) of four tetrodes placed  
989 in the CA1 pyramidal cell layers, as well as plots of standard deviation (SD; bottom). Red  
990 lines indicate  $\pm 3SD$ . C. Individual (grey) and average (red) normalized firing rates from 31  
991 multiunit recordings, 3 consecutive light stimulation epochs are displayed to help visualizing  
992 the consistency of the effect of SuM input light stimulation over area CA2 on CA1 multi-unit  
993 firing; the shaded area represents the SEM. D. Diagram illustrating whole-cell recordings of  
994 area CA1 PNs and SuM fiber light stimulation over area CA2 in acute slice preparation. E-H.  
995 Example waterfall plots (E, G) and corresponding peri-stimulus time histogram (F, H,  
996 population average shown as thick line, shaded area represents SEM) of EPSCs (black) and

- 997 IPSCs (red) recorded from a CA1 PN ex vivo during photostimulation of SuM input over area  
998 CA2 with bath application of 10  $\mu$ M CCh.

999 **Supplemental figure legends**

1000 **Supplemental Figure 1.**

1001 A. Diagram illustrating the intersectional strategy used to label CA2-projecting SuM neurons.  
1002 B – E. Labelling of CA2-projecting SuM neurons with the retrograde CAV-2 carrying Cre-  
1003 recombinase injected in CA2 and the anterograde AAV carrying DIO-EGFP injected in SuM  
1004 of wild type mice. B. Labelling of SuM fibers in the hippocampus from CA2-projecting SuM  
1005 neurons. Left, nissl staining (blue) and EGFP expression (green) in the hippocampus. Right,  
1006 PCP4 staining (magenta) and EGFP expression (green) in area CA2. C. Retrograde-labeled  
1007 SuM neurons that project to hippocampal area CA2. Left, nissl staining (blue) and EGFP  
1008 expression (green) in SuM. Right, calretinin staining (magenta) and EGFP expression (green)  
1009 in SuM. D. Higher magnification image of CA2-projecting SuM neurons. Left, nissl staining  
1010 (blue) and EGFP expression (green) in SuM. Center, nissl (blue) and calretinin staining  
1011 (magenta) in SuM. Right, calretinin staining (magenta) and EGFP expression (green) in SuM.  
1012 E. VGluT2 expression of CA2-projecting SuM neurons. Left, nissl staining (blue) and EGFP  
1013 expression (green) in SuM. Right, VGluT2 staining (red) and EGFP expression (green) in  
1014 SuM. F. Top, diagram illustrating the injection of AAVs into the SuM. Bottom, sagittal image  
1015 of the injection site in SuM to express hCHR2(H134R)-EYFP (green) in the VGluT2-Cre  
1016 line. G and H. Anterograde labelling of SuM projections to the hippocampus from AAV  
1017 carrying DIO-ChR2-EYFP injected in SuM of VGluT2-Cre mice. G. Left, VGluT2 (red) and  
1018 nissl staining (blue) in the hippocampus. Right, hCHR2(H134R)-EYFP -expressing SuM  
1019 fibers (green) and nissl (blue) staining in the hippocampus. H. Left, higher magnification  
1020 image of area CA2 with VGluT2 (red) and nissl (blue) staining. Center, hCHR2(H134R)-  
1021 EYFP -expressing SuM fibers (green) and nissl staining (blue). Right, hCHR2(H134R)-EYFP  
1022 -expressing SuM fibers (green) and VGluT2 staining (red).

1023 **Supplemental Figure 2.**

1024 A. Diagram illustrating the whole-cell recording configuration of PNs in area CA2 and SuM  
1025 fiber stimulation in acute hippocampal slices. B. Light-evoked EPCSs from SuM inputs are  
1026 completely blocked following application of tetrodotoxin (TTX). Sample traces (top, control  
1027 shown in black, +TTX shown in grey) and power-response curves (bottom) of light-evoked  
1028 EPSC amplitudes recorded in PN before (black) and after application of 0.2  $\mu$ M TTX (grey)  
1029 at different light intensities (n = 5, error bars represent SEM). C. Light-evoked EPCSs from  
1030 SuM inputs are completely blocked following application of NMDA and AMPA receptor  
1031 blockers (NBQX & APV). Sample traces (top, control shown in black, NBQX & APV shown

1032 in grey) and time course (bottom) of light-evoked EPSC amplitudes upon application of 10  
1033  $\mu\text{M}$  NBQX & 50  $\mu\text{M}$  APV (n = 6, error bars represent SEM).

1034 **Supplemental Figure 3.**

1035 A. Diagram illustrating the whole-cell recording configuration of PNs in area CA2 and SuM  
1036 fiber stimulation in acute hippocampal slices. B and C. Effect of 10  $\mu\text{M}$  CCh on SuM light-  
1037 evoked PSCs recorded in CA2 PNs under different conditions : voltage clamp at -70 mV with  
1038 inhibitory transmission blocked (B, SR95531 & CGP55845A shown in grey, SR95531 &  
1039 CGP55845A + CCh shown in orange), and voltage clamp at +10 mV (C, control shown in  
1040 red, CCh shown in orange). Left, sample traces. Middle, power-response curves (B, n = 7;  
1041 two-way ANOVA with repeated measures,  $p < 0.001$ ; C, n = 17; two-way ANOVA with  
1042 repeated measures,  $p < 0.001$ ; error bars represent SEM). Right, comparison of PPRs (B, n =  
1043 7; paired-T test,  $p < 0.001$ ; C, n = 17; paired-T test,  $p = 0.001$ ; individual cells shown as grey  
1044 lines, population average shown as horizontal line, error bars represent SEM).

**Table 1. Electrophysiological properties of pyramidal neurons in SuM-innervated area**

	$V_M$ (mV)	$R_M$ (M $\Omega$ )	$C_M$ (pF)
CA2 PN (n = 81)	$-69.8 \pm 0.70$	$59.2 \pm 2.65$	$209 \pm 11.4$
CA3 PN (n = 31)	$-70.3 \pm 1.06$	$72.4 \pm 4.82$	$211 \pm 15.7$
Statistics	Mann-Whitney U test p = 0.997	Student T test p = 0.020*	Mann-Whitney U test p = 0.625
PN deep (n = 57)	$-71.1 \pm 0.76$	$64.0 \pm 3.94$	$200 \pm 12.3$
PN superficial (n = 76)	$-69.3 \pm 0.67$	$64.9 \pm 3.19$	$196 \pm 11.8$
Statistics	Student T test p = 0.077	Mann-Whitney U test p = 0.777	Mann-Whitney U test p = 0.588

**Table 2. Characteristics of SuM light-evoked transmission onto pyramidal neurons**

EPSC						
cell type	connectivity (%)	amplitude (pA)	rise time (ms)	decay time (ms)	latency (ms)	success rate
CA2 PN	56 (n = 58 of 103)	16 ± 1.9	2.9 ± 0.1	14 ± 0.8	2.4 ± 0.2	0.44 ± 0.03
CA3 PN	49 (n = 22 of 45)	23 ± 5.9	3.0 ± 0.2	14 ± 0.9	2.7 ± 0.3	0.56 ± 0.06
Statistics	$\chi^2$ test p = 0.572	Mann-Whitney U test p = 0.409	Mann-Whitney U test p = 0.391	Mann-Whitney U test p = 0.797	Mann-Whitney U test p = 0.156	Student T test p = 0.074
PN deep	56 (n = 35 of 63)	15 ± 2.0	3.5 ± 0.2	16 ± 1.0	3.5 ± 0.4	0.39 ± 0.03
PN superficial	56 (n = 53 of 94)	20 ± 3.0	3.1 ± 0.2	15 ± 0.9	2.7 ± 0.3	0.51 ± 0.04
Statistics	$\chi^2$ test p = 0.946	Mann-Whitney U test p = 0.306	Mann-Whitney U test p = 0.051	Mann-Whitney U test p = 0.314	Mann-Whitney U test p = 0.083	Mann-Whitney U test p = 0.072
IPSC						
cell type	connectivity (%)	amplitude (pA)	rise time (ms)	decay time (ms)	latency (ms)	success rate
CA2 PN	35 (n = 19 of 55)	197 ± 41.3	3.8 ± 0.4	25 ± 1.2	6.3 ± 0.7	0.55 ± 0.06
CA3 PN	57 (n = 16 of 28)	145 ± 23.4	4.5 ± 0.4	25 ± 1.2	7.5 ± 0.9	0.54 ± 0.05
Statistics	$\chi^2$ test p = 0.134	Mann-Whitney U test	Student T test	Mann-Whitney U test	Mann-Whitney U test	Student T test



		p = 0.870	p = 0.203	p = 0.896	p = 0.303	p = 0.893
PN deep	47 (n = 16 of 34)	199 ± 40.6	3.8 ± 0.4	25 ± 1.4	7.2 ± 0.8	0.52 ± 0.07
PN superficial	47 (n = 26 of 55)	167 ± 27.5	4.9 ± 0.4	26 ± 1.2	6.8 ± 0.7	0.50 ± 0.05
Statistics	$\chi^2$ test p = 0.987	Mann-Whitney U test p = 0.258	Student T test p = 0.047*	Student T test p = 0.564	Student T test p = 0.706	Student T test p = 0.796

**Table 3. Electrophysiological properties of interneurons in SuM-innervated area**

	$V_M$ (mV)	$R_M$ (MOhm)	$C_M$ (pF)	firing adaptation index	sag (mV)
Basket cell (n = 16)	$-57.3 \pm 1.38$	$144 \pm 28.1$	$64.0 \pm 8.70$	$0.74 \pm 0.05$	$9.4 \pm 1.0$
non-Basket Cell (n = 12)	$-55.6 \pm 1.84$	$224 \pm 46.8$	$52.0 \pm 5.90$	$0.57 \pm 0.06$	$5.9 \pm 1.4$
interneuron SO (n = 6)	$-57.0 \pm 3.16$	$201 \pm 21.0$	$44.7 \pm 5.31$	$0.61 \pm 0.11$	$7.6 \pm 1.9$
interneuron SR (n = 8)	$-60.1 \pm 2.89$	$282 \pm 49.8$	$39.6 \pm 3.18$	$0.65 \pm 0.09$	$8.1 \pm 2.1$
Statistics	1-way ANOVA test p = 0.527	1-way ANOVA test p = 0.100	Kruskal-Wallis test p = 0.354	1-way ANOVA test p = 0.238	1-way ANOVA test p = 0.292

**Table 4. Characteristics of excitatory SuM light-evoked transmission onto interneurons & pyramidal cells**

cell type	connectivity (%)	amplitude (pA)	rise time (ms)	decay time (ms)	latency (ms)	success rate
Pyramidal Cell	63 (n = 166 of 263)	19 ± 1.6*	3.4 ± 0.1*	15 ± 0.5*	2.9 ± 0.1	0.46 ± 0.02
Basket Cell	82 (n = 18 of 22)	43 ± 8.7*	1.7 ± 0.3*	8.4 ± 1.3*	3.1 ± 0.4	0.59 ± 0.07
non-Basket Cell interneuron SO interneuron SR	39 (n = 10 of 26) 12 (n = 2 of 17) 11 (n = 1 of 9)	16 ± 2.8	2.6 ± 0.5	12 ± 1.4	3.4 ± 0.7	0.36 ± 0.06
Statistics	$\chi^2$ test p = 0.006*	Kruskal-Wallis test p = 0.016 Dunn-Holland-Wolfe post hoc p < 0.05*	1-way ANOVA test p < 0.001 Tukey post hoc p < 0.001*	1-way ANOVA test p < 0.001 Tukey post hoc p < 0.001*	1-way ANOVA test p = 0.580	1-way ANOVA test p = 0.066

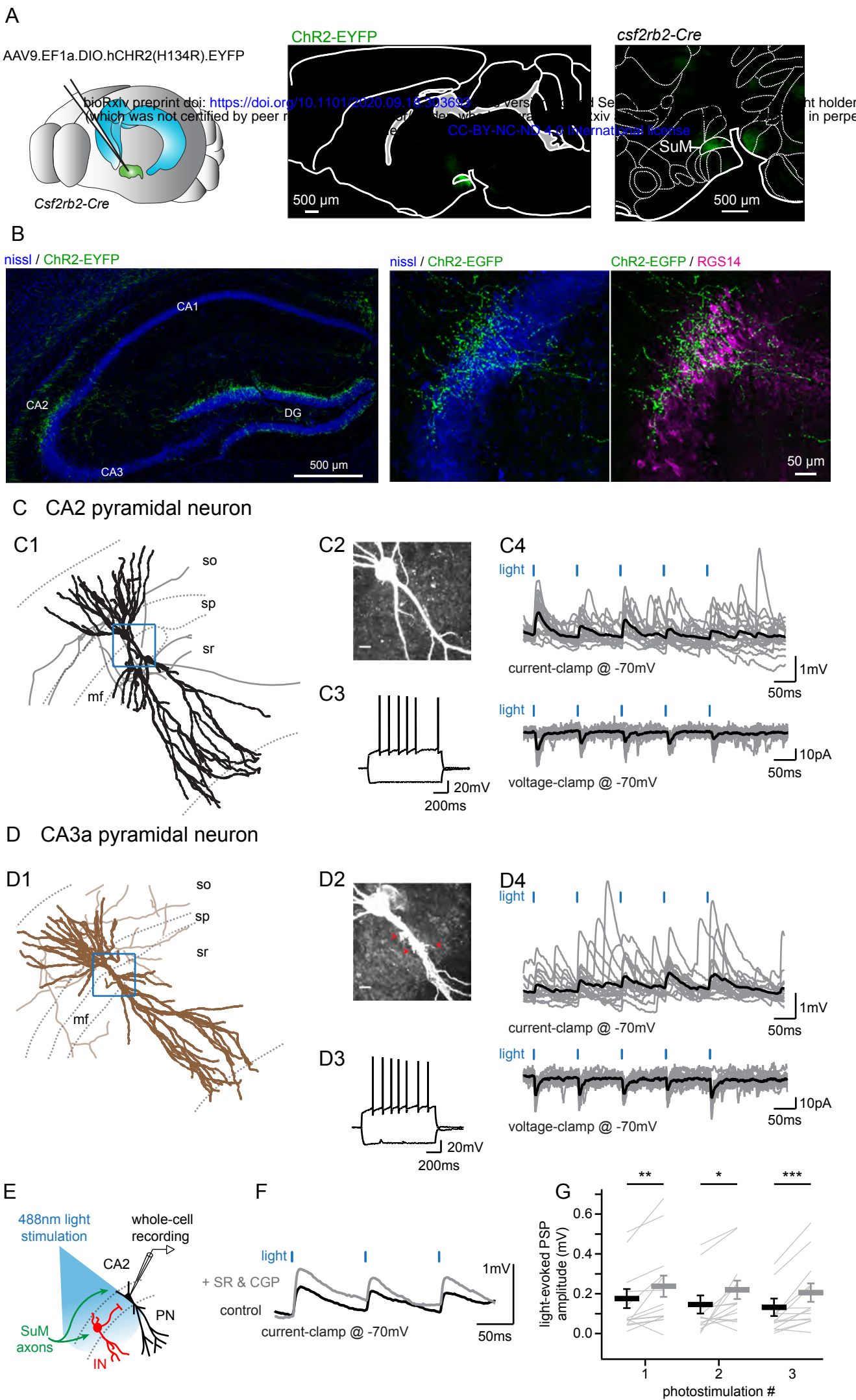
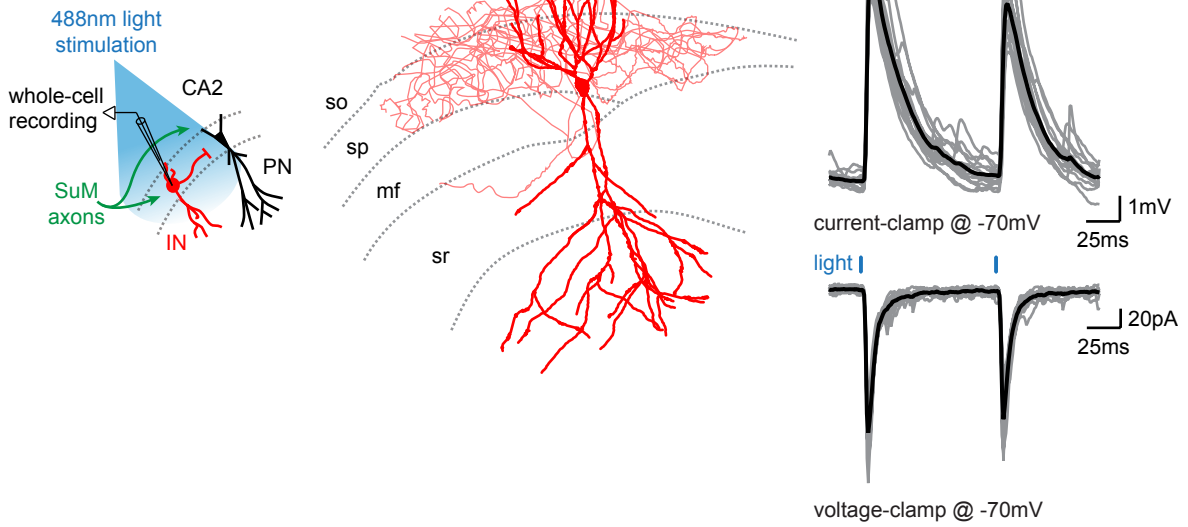


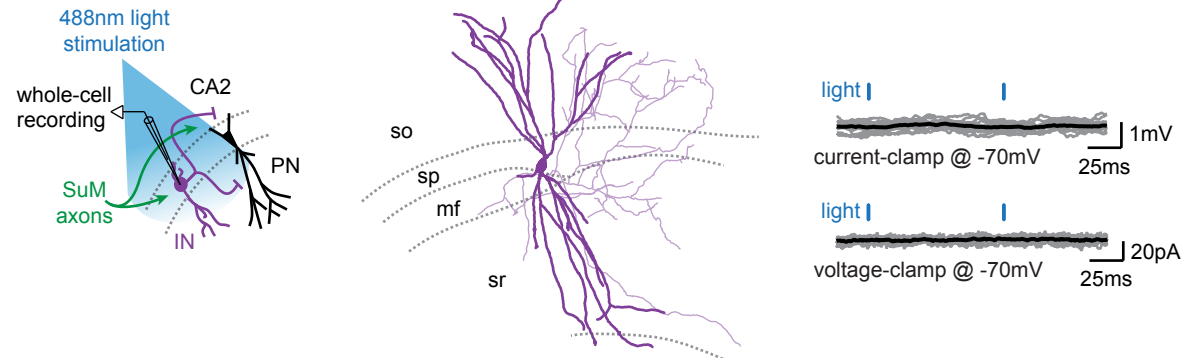
Figure 1.

A

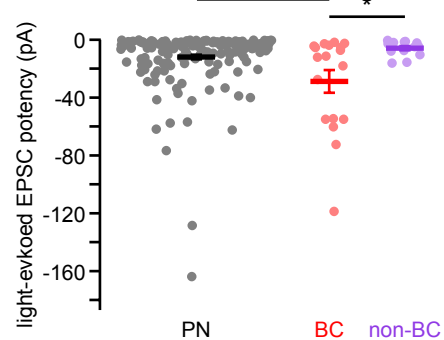
## Basket cells



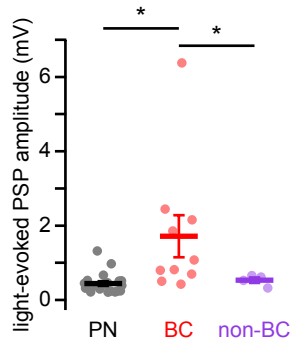
## B Non-basket cells



C



D



E

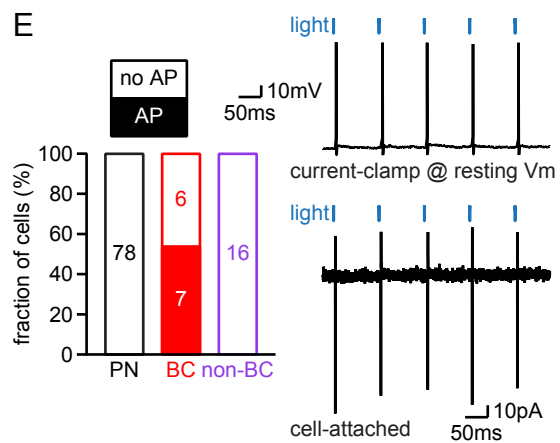


Figure 2.

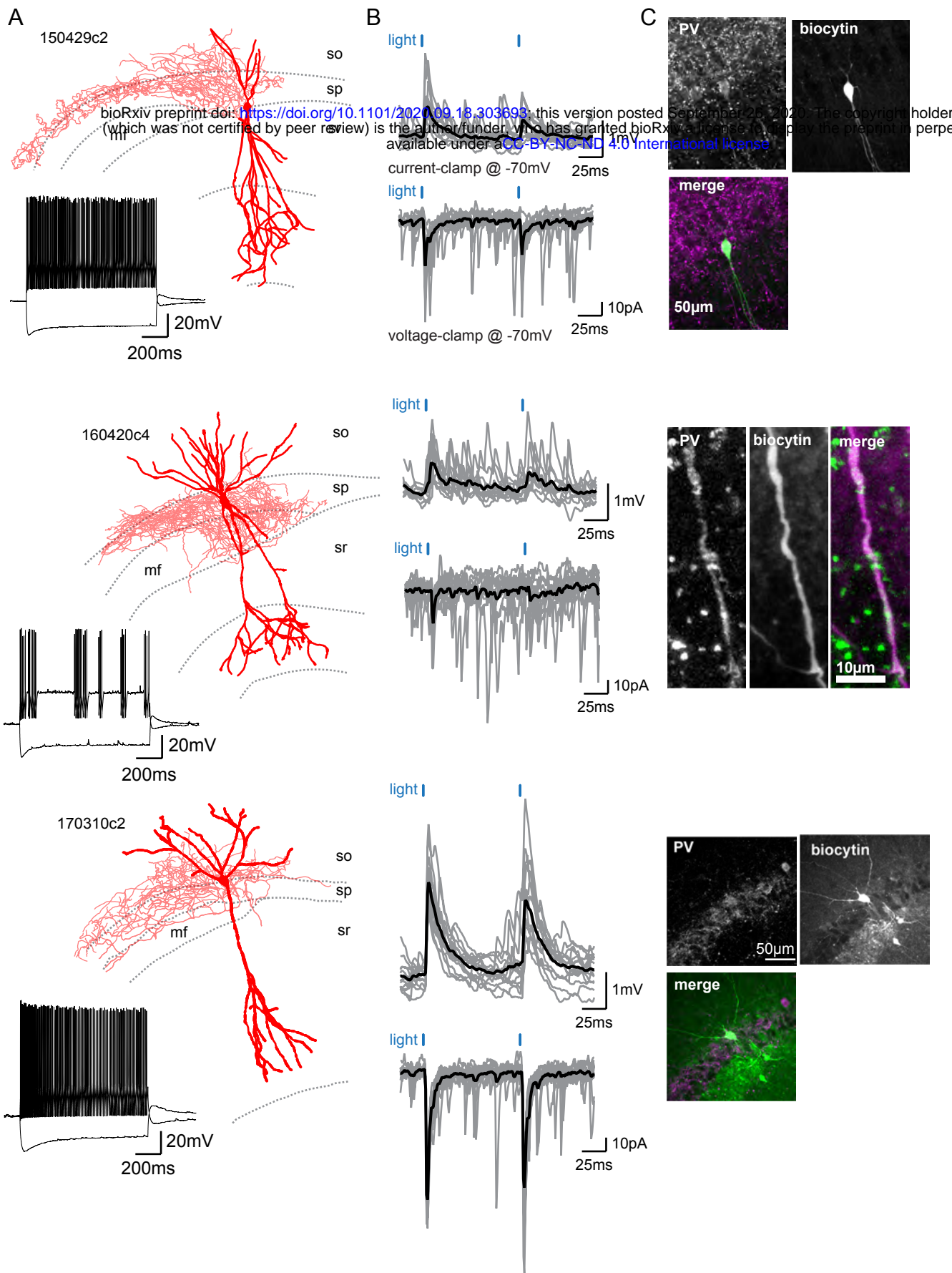


Figure 3.





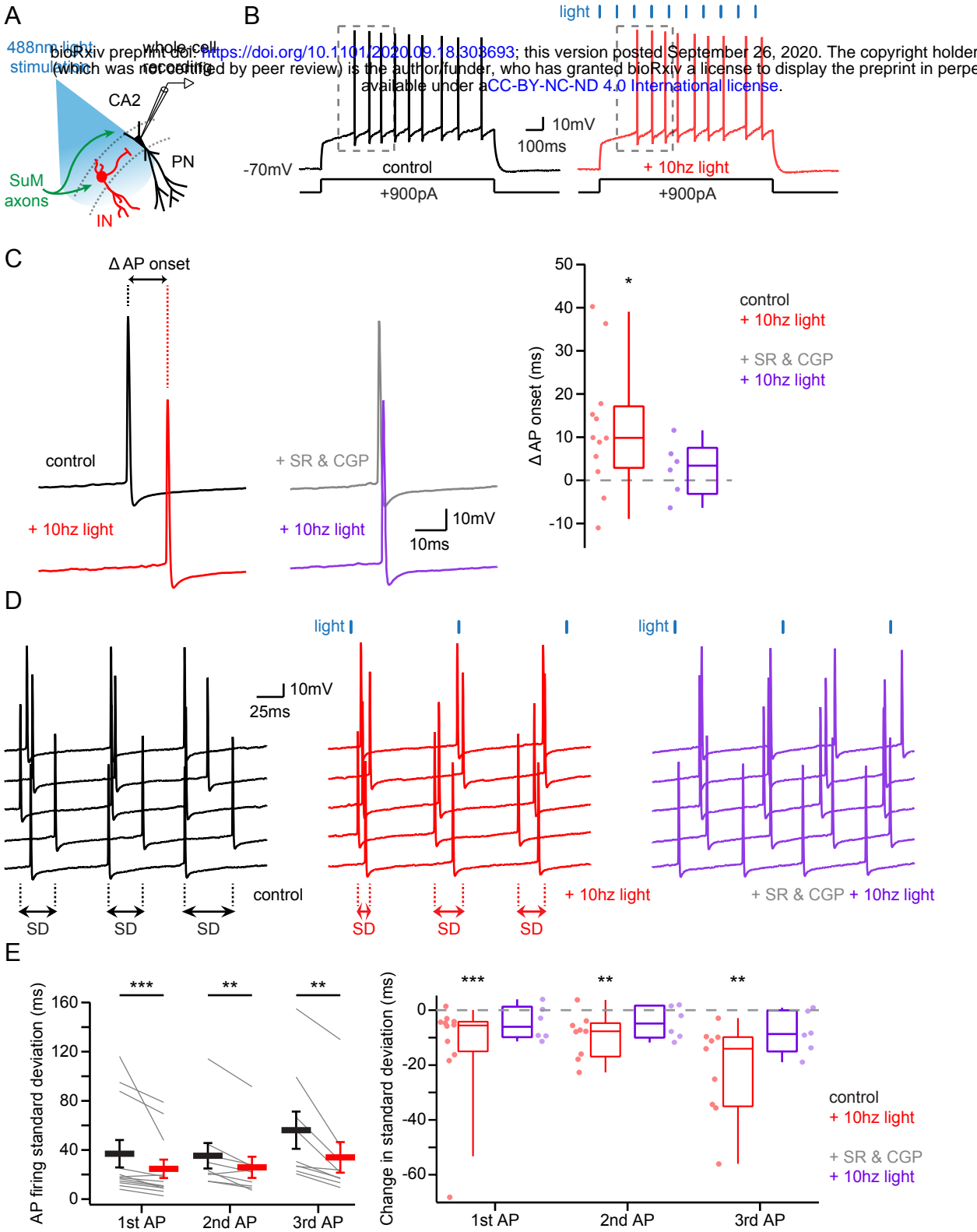


Figure 5.

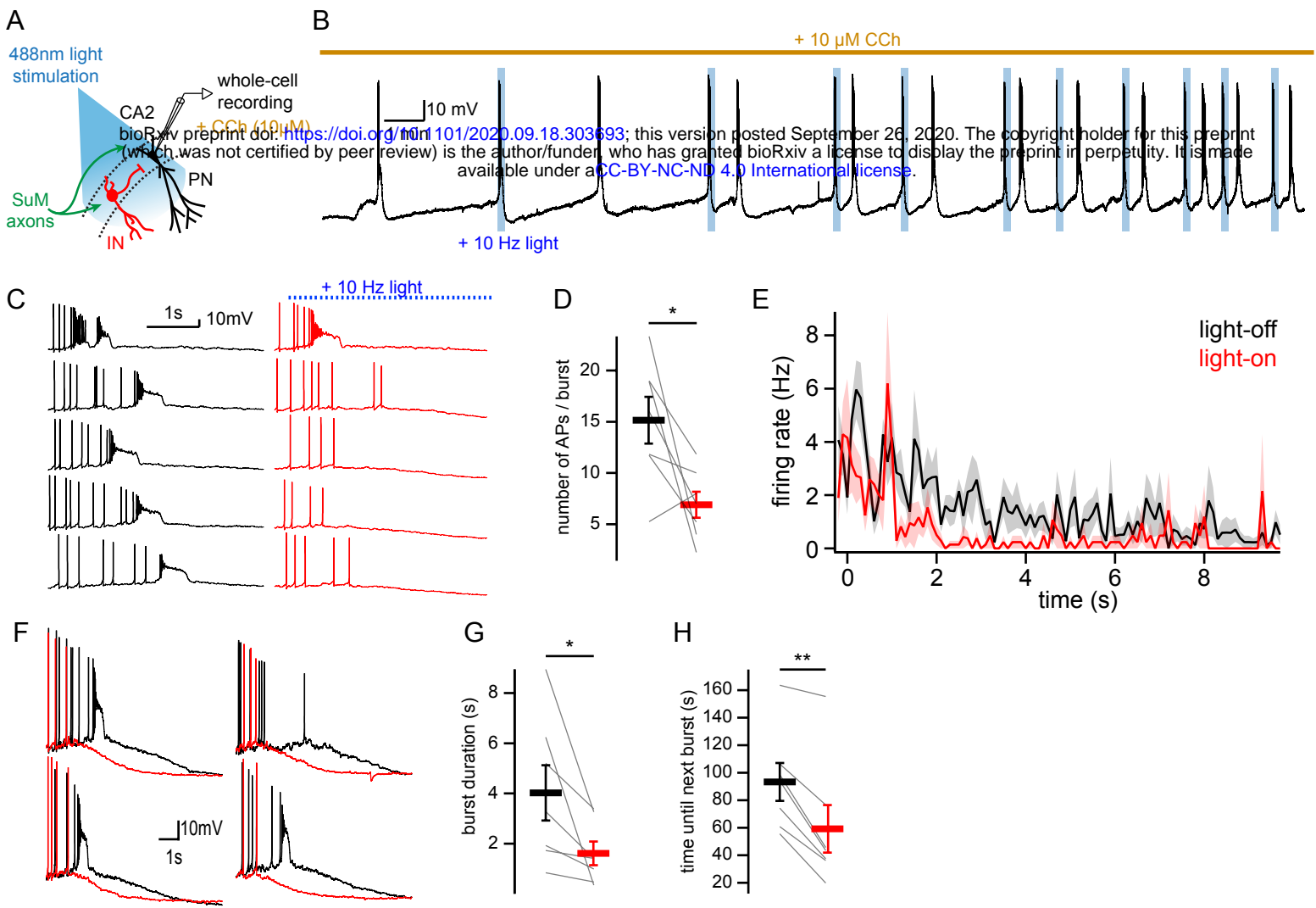


Figure 6.

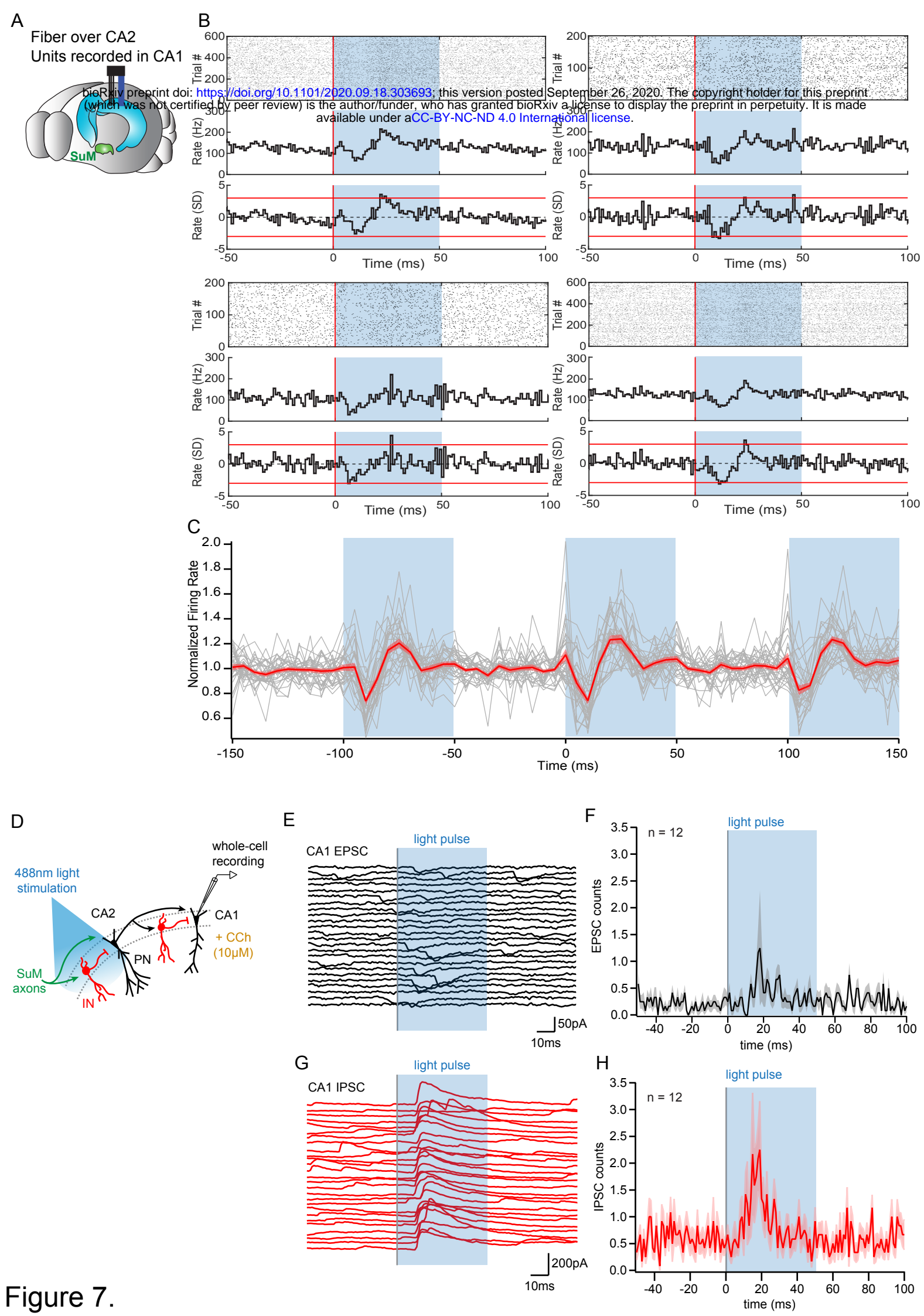
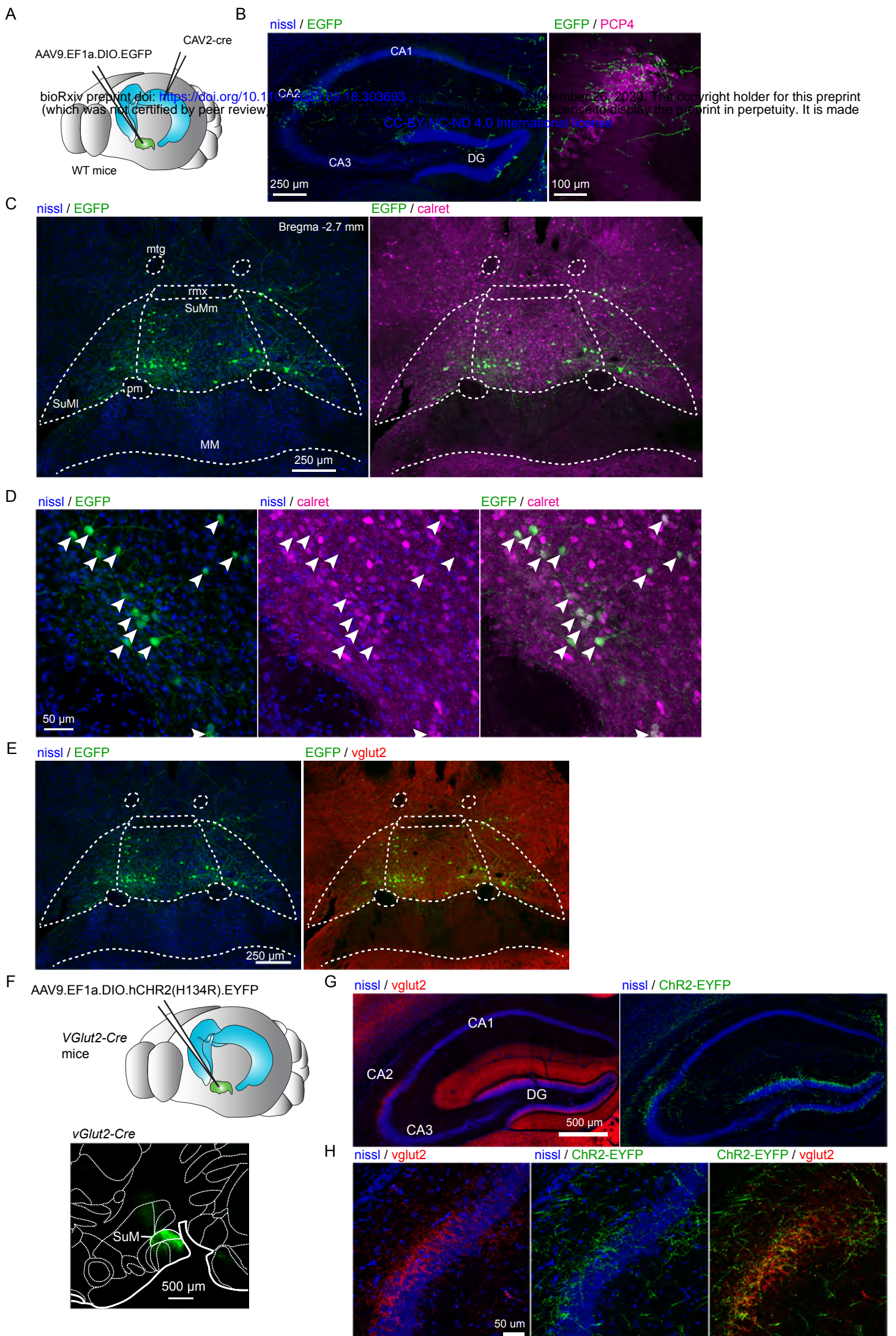


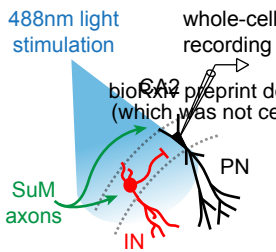
Figure 7.



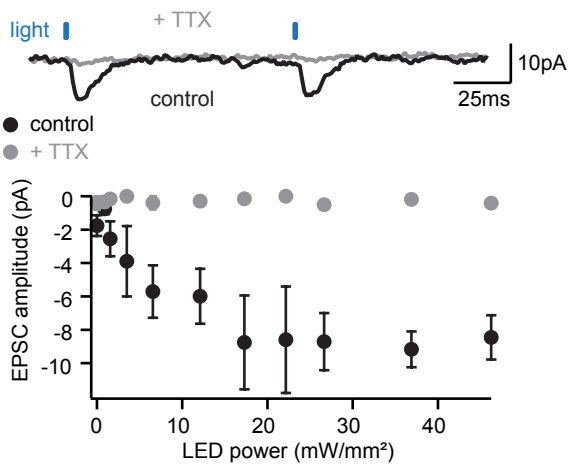


Supplemental Figure 1.

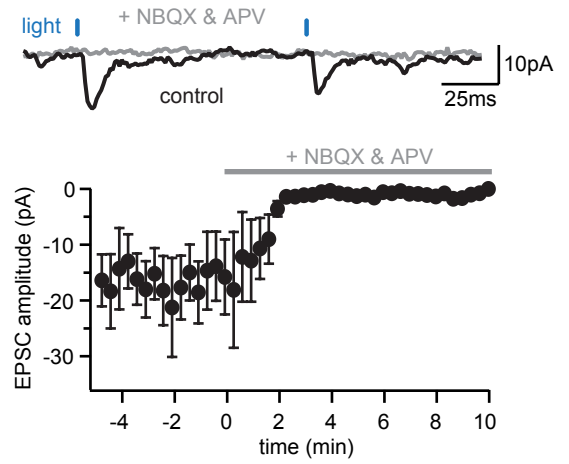
A

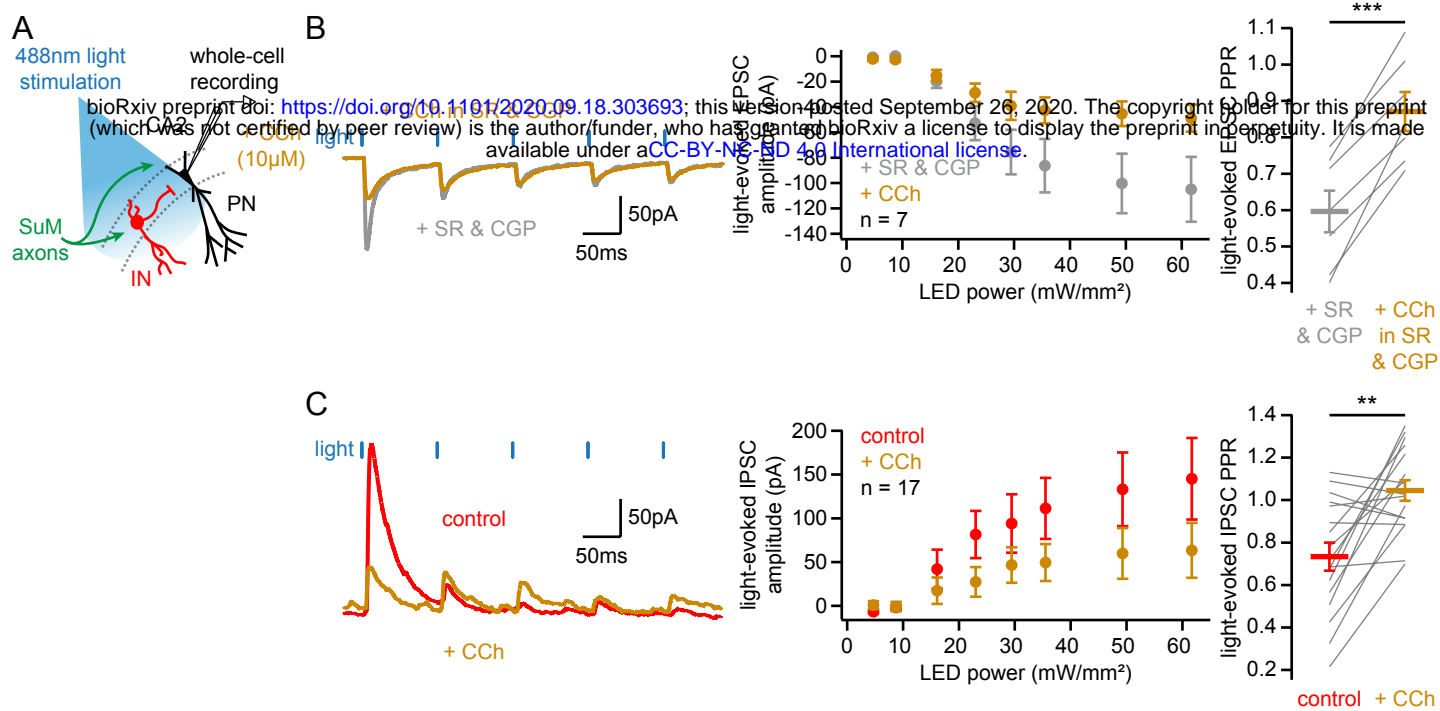


B



C





Supplemental Figure 3.